Organic Geochemistry 187 (2024) 104706

Contents lists available at ScienceDirect

Organic Geochemistry

journal homepage: www.elsevier.com/locate/orggeochem

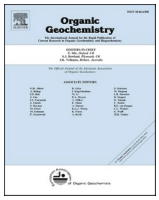

The impact of soil chemistry, moisture and temperature on branched and isoprenoid GDGTs in soils: A study using six globally distributed elevation transects

Cindy De Jonge [a,*], Jingjing Guo [a,b], Petter Hällberg [c], Marco Griepentrog [d], Hamdi Rifai [e], Andreas Richter [f], Edson Ramirez [g], Xinbao Zhang [h], Rienk H. Smittenberg [c,i], Francien Peterse [b], Pascal Boeckx [j], Gerd Dercon [k]

[a] Geological Institute, Earth Science Department, ETH Zurich, Sonnegstrasse 5, 8092 Zurich, Switzerland
[b] Department of Earth Sciences, Utrecht University, Princetonlaan 8A, 3584 CB Utrecht, the Netherlands
[c] Stockholm University, Department of Geological Sciences, and Bolin Center for Climate Research, Sweden
[d] Soil Resources, Department of Environmental Systems Science, ETH Zurich, Universitätstrasse 16, 8092 Zurich, Switzerland
[e] Department of Physics, Faculty of Mathematics and Natural Sciences, Universitas Negeri Padang, Indonesia
[f] Centre for Microbiology and Environmental Systems Science, University of Vienna, Djerassiplatz 1, 1030 Vienna, Austria
[g] Universidad Mayor de San Andres Bolivia, La Paz, Bolivia
[h] Institute of Mountain Hazards and Environment, Chinese Academy of Sciences, Chengdu 610299, China
[i] Now at Swiss Federal Institute for Forest, Snow and Landscape Research WSL, Birmensdorf, Switzerland
[j] Isotope Bioscience Laboratory – ISOFYS, Department of Green Chemistry and Technology, Ghent University, Gent, Belgium
[k] Soil and Water Management and Crop Nutrition Laboratory, Joint FAO/IAEA Centre of Nuclear Techniques in Food and Agriculture, Friedensstrasse 1, 2444 Seibersdorf, Austria

ARTICLE INFO

Communicated by Steven John Rowland

ABSTRACT

Glycerol dialkyl glycerol tetraethers (GDGTs) are microbial membrane-spanning lipids that are produced in a variety of environments. To better understand the potentially confounding effect of soil chemistry on the temperature relationship of branched GDGTs (brGDGTs), isoprenoid GDGTs (isoGDGTs) and GDGT-based proxies MBT'$_{5ME}$ and TEX$_{86}$, soils from 6 elevation transects (mean annual air temperature 0 – 26 ℃, n = 74) were analyzed. Corroborating earlier work, the MBT'$_{5ME}$ index correlates well with mean annual air temperature in the low pH (pH < 7), non-arid soils under study (r = 0.87, p < 0.001). However, a clear over-estimation of reconstructed temperature in the lowest pH (<3.5) soils is observed, explained by the correlation between brGDGT Ia and free acidity. TEX$_{86}$ also shows a significant correlation with mean annual air temperature (r = 0.45, p < 0.001), driven by temperature dependent concentration changes of isoGDGTs 3 and cren'. However, an overarching correlation with P/E values dominates concentration changes of all supposed Thaumarchaeotal isoGDGTs lipids (GDGT1-3, cren and cren'), implying a potential impact of soil moisture on TEX$_{86}$ values. In addition to identifying the impact of these confounding factors on the temperature proxy, GDGT ratios that can be used to constrain changes in soil chemistry, specifically exchangeable Ca^{2+}, sum of basic cations, exchangeable Fe^{3+} and sum of soil metals are proposed ($0.53 < r^2 < 0.68$), while existing ratios for soil moisture availability are tested for the first time in a dataset of non-arid soils. While the impact of soil chemistry on GDGTs may complicate the interpretation of their temperature proxies, our proposed GDGT ratios can potentially be used to constrain a subset of soil chemistry changes through time.

1. Introduction

GDGTs are membrane-spanning lipids that are produced in a variety of environments. In soils, branched GDGTs (brGDGTs; Supp. Fig. 1) are abundant lipids produced by a possibly large diversity of bacterial producers (e.g., Sinninghe Damsté et al., 2018; De Jonge et al., 2019; Guo et al., 2022). Based on both environmental distributions (Weijers et al., 2009) and cultured representatives (Sinninghe Damsté et al.,

* Corresponding author.
E-mail address: cindy.dejonge@erdw.ethz.ch (C. De Jonge).

https://doi.org/10.1016/j.orggeochem.2023.104706
Received 14 July 2023; Received in revised form 16 November 2023; Accepted 20 November 2023
Available online 22 November 2023

2011, 2014, 2018; Halamka et al., 2021, 2023; Chen et al., 2022), Acidobacteria are proposed as important producers in soils. Contributions from other soil bacteria can however not be ruled out, as the genetic potential to form membrane-spanning lipids is widespread in bacteria (Sahonero-Canavesi et al., 2022; Zeng et al., 2022). On a global scale, a relative increase of brGDGT Ia and decrease of brGDGT IIa and IIIa (Supp. Fig. 1 for structures) is observed with increasing temperature, which forms the basis of the paleotemperature proxy MBT (methylation index of branched tetraethers; Weijers et al., 2007), MBT' (simplified MBT; Peterse et al., 2012) and the modified MBT'$_{5ME}$, that has been correlated against mean annual air temperature (Air MAT; e.g., De Jonge et al., 2014a) or Air MAT based on days without freezing (BayMBT$_0$ calibrated against MAT$_0$; Dearing Crampton-Flood et al., 2020). In addition, temperature calibrations can be based on a linear combination of the fractional abundance of brGDGTs (e.g., Raberg et al., 2021; Véquaud et al., 2021).

Elevation transects, that cover a large temperature range over a smaller spatial scale, have been used extensively to test the performance of the MBT$^{(')}$ and MBT'$_{5ME}$ temperature proxies. Significant correlations between elevation (or temperature) and i) the brGDGT ratios MBT$^{(')}$/CBT (where CBT stands for Cyclization of Branched Tetraether index; Weijers et al., 2007; Sinninghe Damsté et al., 2008; Peterse et al., 2009; Yang et al., 2010; Loomis et al., 2011; Liu et al., 2013; Ernst et al., 2013; Coffinet et al., 2014, 2017; Anderson et al., 2014; Yang et al., 2015a; Wang et al., 2017a), MBT'$_{5ME}$ (Yang et al., 2015b; Wang et al., 2018; Duan et al., 2020; Véquaud et al., 2021), or ii) the reconstructed mean annual temperature values using MAT$_{mr}$ (Nieto-Moreno et al., 2016; Jaeschke et al., 2018; Kirkels et al., 2020) based on a multiple linear regression (De Jonge et al., 2014a) and the BayMBT$_0$ (van der Veen et al., 2020) are reported. Still, several studies report offsets between MBT ratios and temperature and/or elevation when vegetation, soil type, soil moisture, seasonality or slope aspect changes (Sinninghe Damsté et al., 2008; Peterse et al., 2009, Loomis et al., 2011; Anderson et al., 2014; Wang et al., 2017a; Wang et al., 2018; Duan et al., 2020). Also, while the proposed pH proxy CBT generally traces pH well, it has also been observed to change with elevation ($r^2 < 0.50$) independently of soil pH (Coffinet et al., 2014). This suggests that unknown edaphic parameters influence brGDGTs. We hypothesize that soil chemistry parameters can be a confounding factor, as their impact on GDGT concentrations and ratio values is generally not tested in these settings. This hypothesis reflects the recent insight that MBT'$_{5ME}$ values in soils can be directly influenced by uniquely pH (De Jonge et al., 2021), or both temperature and pH (Dearing Crampton-Flood et al., 2020; Véquaud et al., 2021; Halffman et al., 2022). So far, only two elevational transect studies have included soil chemistry parameters, and both concluded that soil pH has a direct impact, firstly on temperature-sensitive brGDGTs in the French Alps (Véquaud et al., 2021, $3.6 < pH < 7.6$) and secondly on MBT'$_{5ME}$ values in subarctic low pH soils ($3.3 < pH < 5.7$, Halffman et al., 2022).

A second group of compounds, isoprenoid GDGTs (isoGDGTs), are produced by archaea. Individual isoGDGTs have a wide or narrow taxonomic specificity: isoGDGTs with zero to three cyclopentane moieties (GDGT 0–3), are compounds produced by a wide diversity of archaea (excluding halophilic Archaea; Schouten et al., 2013), while crenarchaeol, containing one cyclohexane and four cyclopentane moieties, is a specific marker for Thaumarchaeota (Sinninghe Damsté et al., 2002). In most soils, the phylogenetic Thaumarchaeotal lineage I.1b is dominant over the lineage I.1a (Auguet et al., 2010; Bates et al., 2011). As Thaumarchaeota are dominant ammonia oxidizers in low pH soils (Ammonia-Oxidizing Archaea: AOA, Nicol et al., 2008), their lipids can potentially be used to quantify the abundance of ammonia oxidizers (Leininger et al., 2006). IsoGDGTs have been used only sparsely as environmental proxies in soils, although they are at the base of the popular TEX$_{86}$ proxy (tetraether index of 86 carbon atoms) for sea surface temperature (Schouten et al., 2002; Tierney and Tingley, 2015). In spite of the lower research intensity, TEX$_{86}$ values in soils have also been found to vary with Air MAT, decreasing with elevation at Mt. Xiangpi and Mt. Jianfengling in China (Liu et al., 2013; Yang et al., 2010; 2016), at Mt. Rungwe in Tanzania (Coffinet et al., 2014), along Mt. Tienshan and in Northern Iran (Duan et al., 2022), and on a global scale with Air MAT and/or soil moisture (Yang et al., 2016). This temperature dependency in globally distributed soils matches temperature-driven changes in TEX$_{86}$ values in cultures of soil-derived archaeal strains (Sinninghe Damsté et al., 2012). However, Dirghangi et al. (2013) and Yang et al. (2016) illustrate across three climatic transects in China and USA that TEX$_{86}$ and Air MAT are not always correlated significantly, with changes in the archaeal community (reflecting either oxic or anoxic soil conditions) proposed to be a confounding factor (Duan et al., 2022).

Based on global or local calibrations, both branched and isoprenoid GDGT distributions, sampled from loess-paleosol sequences (e.g., Peterse et al., 2011; Duan et al., 2022), paleosol (Yamamoto et al., 2016) and lignite archives (e.g., Inglis et al., 2017; Lauretano et al., 2021), have been used to reconstruct local changes in temperature, soil pH and/or soil moisture. To test the hypothesis that soil chemical parameters influence the distribution of GDGTs, the effect of soil chemistry and temperature on the concentration and distribution of 15 brGDGTs and 6 isoGDGTs was investigated in a dataset of 6 globally distributed elevation transects.

Here, we expand on the approach to use elevation transects to capture large temperature gradients, while also accounting specifically for changes in soil chemistry across and between transects. Based on this dataset, we identify which GDGTs and ratios are influenced by soil chemistry. To potentially constrain large changes in soil chemistry through time, new GDGT ratios for selected soil parameters -mean annual precipitation (MAP), sum of exchangeable base cations (including exchangeable calcium) and exchangeable metals (including iron)- are proposed. Development of these ratios will enable us to recognize large changes in soil chemistry over time that may alter the temperature relationship of the GDGTs, and ultimately improve the reliability of the MBT'$_{5ME}$ and TEX$_{86}$ proxies in paleosol and lignite archives.

2. Materials and methods

2.1. Elevation transects and climate parameters

The six elevation gradients under study are located in 5 different countries: Austria, Mt Rauris ($n_{samples} = 12$); Bolivia, Mt Zongo ($n_{samples} = 8$); China, Mt. Gongga ($n_{samples} = 8$); Indonesia (2 transects: Mt. Singgalang (SG, $n_{samples} = 24$) and Transect to Coast (TC, $n_{samples} = 14$)) and Tanzania, Mt. Kilimanjaro ($n_{samples} = 8$). In addition to being located in different climate zones (temperate to tropical), the elevation differences (Supp. Table 1) covered at each location add additional temperature variation. Most of the higher elevations are dominated by grassland, while the lower elevation areas are dominated by forest, except for Tanzania, where the lower elevation area was dominated by savanna (Supp. Table 1). An exception is the Indonesian transect (TC and SG transects), which is forested along the complete elevation transect (Hällberg et al., 2023). Soil moisture at the time of sampling had not been quantified, but descriptions reflect soils that were neither dry nor waterlogged during sampling and are not characterized as peats. As soils from Austria, Bolivia, China and Tanzania are collected through the regional Technical Cooperation Project INT5153, from the International Atomic Energy Agency (IAEA), they are referred to as "IAEA" soils in the methods section.

Mean annual air temperatures (Air MAT) for each sample location have been extracted from the CHELSA database (long-term annual means (1973–2013) downscaled at a 1 km resolution, Karger et al., 2017). In addition, the Growing Season Temperature (Air GST) was extracted, which reflects the air temperature of the growing season, whose length is constrained by snowpack and drought (Treelim, based on WorldClim 1970–2000 climate data; Paulsen and Korner, 2014). As

the GDGT producers experience soil temperature, which can be offset from air temperature (Wang et al., 2020; Halffman et al., 2022; Lembrechts et al., 2022), mean annual soil temperature (Soil MAT) and mean soil temperatures of the warmest quarter (i.e., soil mean summer temperature, Soil MST) are extracted from the SoilTemp database (reflecting measurements done between 2000 and –2020; Lembrechts et al., 2022), both for the top 5 cm of the soil column. For the Indonesian Singgalang transect, that is located along a very steep gradient, the spatial resolution in CHELSA and SoilTemp was insufficient, and we performed a correction of the air and soil temperatures based on elevation (Supp. Fig. 2). The resulting CHELSA-derived Air MAT lapse rate (0.55 ℃ per 100 m) is close to published lapse rates at this location (0.56–0.58; Nishimura et al., 2006), indicating that our approach captures the temperature variability along Mt. Singgalang accurately. Mean monthly precipitation (MMP) and actual evapotranspiration (AET) at each location was extracted from the TerraClimate database (4 km resolution, period between 1958 and 2021; Abatzoglou et al., 2018) and averaged to get a yearly mean. The ratio calculated and reported here (MMP/AET = P/E) is interpreted as an indicator for soil moisture availability (Hobbins et al., 2016).

2.2. Soil chemistry parameters

All soils were sieved over a 2 mm sieve and homogenized in a ball mill, before subsampling for EA-IRMS. For the Indonesian soils, the total carbon (TC), total nitrogen (TN), $\delta^{13}C$ and $\delta^{15}N$ were measured on an Elemental Analyzer (Flash-EA 1112, ThermoFisher Scientific) coupled to an isotope ratio mass spectrometer (IRMS, Delta V, ThermoFisher Scientific) at the Geological Institute, ETH Zürich. TC and TN contents are reported in percent (%) of dry weight soil. As the contribution of inorganic carbon is negligible in non-arid and low pH soils (Lal, 2017), TC and TOC are considered equal for the purpose of this study. For $\delta^{13}C$ and $\delta^{15}N$, calibration was done using atropine ($\delta^{13}C$ = -21.4; $\delta^{15}N$ = -2.9), peptone ($\delta^{13}C$ = -15.64, $\delta^{15}N$ = 6.67) and nicotinamide ($\delta^{13}C$ = -42.2, $\delta^{15}N$ = -1.99) standards with known carbon and nitrogen content and isotopic composition. The reproducibility of the isotope measurements was better than 0.2 ‰ for both elements. The IAEA soils were measured on an elemental analyzer (ANCA-GSL, SerCon) interfaced with an IRMS (20–22 with SysCon electronics, SerCon) using a SerCon soil as standard (accepted value $\delta^{13}C$ VPDB = –22.69 ± 0.3 ‰ and $\delta^{15}N$ AIR = +7.81 ± 0.2 ‰) at ISOFYS, Ghent University. Again, TC and TN contents are reported in percent (%) of dry mass soil.

For all sieved soils (2 mm sieve), pH was measured in a 1 M KCl solution (soil: solution ratio, 1:5, w/v) after 10 min of shaking and 1 h of sedimentation. Exchangeable cations were measured after extraction of the milled soil in 1 M ammonium acetate (pH = 7). The titration curve was determined using 50 mL of 1 M ammonium acetate at pH 7 and subsequent titration with 0.1 N acetic acid while noting the decrease in pH. The concentration of free hydrogen ions (free acidity) was calculated back based on a titration curve (Brown, 1943). Exchangeable cations: K^+, Na^+, Mn^{2+}, Ca^{2+}, Mg^{2+}, Al^{3+}, Fe^{3+}, were measured using Inductively Coupled Plasma Optical Emission Spectroscopy (ICP-OES). The Cation Exchange Capacity (CEC) is calculated as $H^+ + Na^+ + K^+ + 2Ca^{2+} + 2Mg^{2+} + 3Al^{3+}$ (all in cmolc kg $soil^{-1}$), Σbases is calculated as $Na^+ + K^+ + 2Mg^{2+} + 2Ca^{2+}$ (all in cmolc kg $soil^{-1}$). Σmetals is calculated as $3Fe^{3+} + 2Mn^{2+} + 3Al^{3+}$ (all in cmolc kg $soil^{-1}$), while base saturation (%) is calculated as (($Na^+ + K^+ + 2Ca^{2+} + 2Mg^{2+}$ (all in cmolc kg^{-1} soil))/CEC)*100.

2.3. GDGT extraction and analysis

Between 1 and 5 g of dry IAEA soil was extracted using an Energized Dispersive Extraction (EDGE) instrument, using dichloromethane (DCM): methanol (MeOH) 9: 1 (v/v) at 110 °C to obtain a total lipid extract (TLE). After addition of 100–200 ng of internal standard (Huguet et al., 2006), the TLEs were subsequently dried under a gentle N_2 stream and separated into apolar, ketone and polar fractions by passing them over an activated Al_2O_3 column using hexane: DCM (9: 1, v/v), hexane: DCM (1: 1, v/v) and DCM: MeOH (1: 1, v/v), as elution solvents, respectively. The polar fractions, containing GDGTs, were dried under a N_2 stream and re-dissolved into a hexane: isopropanol (99: 1, v/v) solution, and filtered through a 0.45 μm PTFE filter. The GDGTs were analyzed with an Agilent 1260 Infinity ultra high performance liquid chromatograph (viz by UHPLC), coupled to an Agilent 6130 single quadrupole mass spectrometer, using the method described in Hopmans et al. (2016), with the modification that columns are kept at 45 ℃. This allowed separation and integration of 6 isoprenoid GDGTs (*m/z* 1300, 1298, 1296, 1292), 15 brGDGT compounds (*m/z* 1022, 1020, 1018, 1036, 1034, 1032, 1050, 1048, 1046), and an internal standard (*m/z* 744). Concentrations are based on the peak areas of individual GDGTs and the internal standard, corrected for g of soil extracted. Based on a long-term laboratory standard the analytical uncertainty is 0.02 for MBT'_{5ME} and 0.03 for IR values.

For the Indonesian transects SG and TC, 1–2 g of freeze-dried and ground soil was extracted by over-night acid hydrolysis (45 °C), using a mixture of MeOH and hydrochloric acid (HCl, 35 % w/w) (1:3 v/v). The lipids were recovered from the organic phase after addition of equal amounts of DCM and pre-extracted Milli-Q water, followed by sonication (15 min), centrifugation and pipetting off the organic DCM layer (3x). The TLE was acid neutralized by adding a scoop of Na_2CO_3 and dried under a gentle N_2 stream, redissolved into DCM and adsorbed to a small amount of silica gel (deactivated with 5 % H_2O) which was subsequently air-dried and placed on top of a silica gel column. The TLE was fractionated into an apolar and a polar fraction by eluting with hexane and DCM: MeOH (1: 1, v/v), respectively. After drying, the polar fraction was redissolved in hexane: isopropanol (99: 1 v/v) which was filtered through a 0.45 μm PTFE filter. GDGTs were analyzed using the method described by Hopmans et al. (2016), except for using a flow of 0.3 mL min^{-1} and a slightly adjusted solvent gradient, on a Dionex/Thermo Scientific UltiMate3000 HPLC (equipped with two Acquity UPLC HILIC columns, 2.1 x 150 mm) connected to a TSQ Quantum Access Max Triple Quadrupole mass spectrometer and APCI ion source. GDGTs were scanned using *m/z* windows 1017–1023, 1031–1037, 1045–1051 and 1290–1304. The relative abundances of isoprenoid and branched GDGTs were manually integrated using the Xcalibur software package. To validate the extraction protocol described above, eight soils were also extracted in a similar way to the IAEA soils, by sonication with DCM: MeOH 9: 1 (v/v) without prior acid hydrolysis, and this gave no significantly different results.

The GDGT ratios are calculated following De Jonge et al., 2014a (MBT'_{5ME}, CBT') and De Jonge et al., 2014b (IR [Isomer Ratio]), while the DC' (Degree of Cyclization) is modified after Sinninghe Damsté et al., (2009). fIa_{Meth}, fIb_{Meth} and fIc_{Meth} are calculated after Raberg et al. (2021). IsoGDGT ratios are calculated after Schouten et al. (2002) (TEX_{86}) and Baxter et al., 2021 (f[CREN']). To allow comparison of isoGDGT and brGDGT concentrations, the BIT (Branched and Isoprenoid Tetraether) index follows Hopmans et al. (2004), explicitly including 6-methyl brGDGTs, and the Ri/b is calculated as in Xie et al. (2012). GDGT structures are shown in Supp. Fig. 1:

$$MBT'_{5ME} = (Ia + Ib + Ic)/(Ia + Ib + Ic + IIa + IIb + IIc + IIIa) \quad [Eq.\ 1]$$

$$CBT' = {}^{10}\log((Ic + IIa'+IIb'+IIc'+IIIa'+IIIb'+IIIc')/(Ia + IIa + IIIa)) \quad [Eq.\ 2]$$

$$IR = (IIa'+IIIa')/(IIa + IIIa + IIa'+IIIa') \quad [Eq.\ 3]$$

$$DC' = (Ib + IIb + IIb')/(Ia + IIa + IIa'+Ib + IIb + IIb') \quad [Eq.\ 4]$$

fIx_{Meth} = Ix/(Ix + IIx + IIIx), with x denoting either a, b or c compounds (Supp. Fig. 1) [Eq. 5]

$$TEX_{86} = (GDGT2 + GDGT3 + cren')/ (GDGT1 + GDGT2 + GDGT3 + cren') \quad [Eq.\ 6]$$

$$f[CREN'] = cren'/(cren'+cren) \quad [Eq.\ 7]$$

$$BIT = (Ia + IIa + IIIa + IIa'+IIIa')/(Ia + IIa + IIIa + IIa'+IIIa'+cren) \quad [Eq.\ 8]$$

$$Ri/b = \Sigma isoGDGTs/\Sigma brGDGTs \quad [Eq.\ 9]$$

The performance of modified temperature calibrations proposed in this manuscript (Calibration A-D and Eq. 10) is tested using a dataset of global soils and peats published by Dearing Crampton-Flood et al. (2019). MBT'$_{5ME}$, IR and Air MAT values are extracted from the same database, Air GST values are extracted from CHELSA, based on the published coordinates.

2.4. Statistical approaches

To describe environmental drivers on concentration changes, linear correlations coefficients (pearson r-value) are reported for those correlations with $p \leq 0.05$. An unconstrained principal component analysis (PCA), based on standardized fractional abundances of i) 11 brGDGTs (excluding compounds IIc, IIc', IIIc and IIIc') or ii) 6 isoGDGTs, is used to visualize explained variance. Environmental variables are plotted *a posteriori* in the ordination space. A redundancy analysis (RDA), in combination with an automatic stepwise model building approach is used to determine the environmental variables that explain a significant amount of the GDGT variance, and the unique fraction of variance explained by each of these parameters is determined using a partial RDA (pRDA). The accuracy of calibration is reported using the RSME (residual standard mean error) and the squared Pearson correlation coefficient. To correct for the influence of pH on the temperature dependency of the MBT'$_{5ME}$ values, the IR (a brGDGT-based ratio that correlates with soil pH), is included as a second explanatory variable in the multiple linear regression model of the form $MAT = a + b*MBT'_{5ME} + c*IR$. The statistical approach to find the lipid ratios that correlate best with environmental variables, is outlined in Peterse et al. (2012) and De Jonge et al., (2014a). Here, brGDGTs IIIc and IIIc' were excluded, as

Table 1
Correlation between air mean annual temperature (Air MAT), air growing season temperature (Air GST), soil mean annual temperature (Soil MAT), and soil mean summer temperature (Soil MST), climate (MMP: mean monthly precipitation), AET (actual evapotranspiration), P/E (precipitation/evaporation ratio) and chemical variables.

	Air MAT (°C)	Air GST (°C)	Soil MAT (°C)	Soil MST (°C)	Air MAT (°C)
Air MAT (°C)	/	<0.001	<0.001	<0.001	/
range: 0.3–26.4	/	0.94	0.98	0.84	/
Air GST (°C)	<0.001	/	<0.001	<0.001	<0.001
range: 5.0–27.0	0.94	/	0.97	0.94	0.94
Soil MAT (0–5 cm, °C)	<0.001	<0.001	/	<0.001	<0.001
range: 1.0–25.0	0.98	0.97	/	0.92	0.98
Soil MST (0–5 cm, °C)	<0.001	<0.001	<0.001	/	<0.001
range: 6.0–25.3	0.84	0.94	0.92	/	0.84
MMP (mm/month)	<0.001	<0.001	<0.001	<0.001	<0.001
range: 60–326	0.58	0.63	0.54	0.39	0.58
AET (mm/month)	<0.001	<0.001	<0.001	<0.001	<0.001
range: 32–113	0.91	0.84	0.86	0.66	0.91
P/E	<0.05		<0.05		<0.05
range: 1.1–4.3	−0.27		−0.26		−0.27
Soil pH	<0.05	<0.01	<0.01	<0.001	<0.05
range: 2.5–6.7	0.23	0.32	0.31	0.44	0.23
$\delta^{15}N$ (‰)					
range: −1.5–8.5					
$\delta^{13}C$ (‰)	<0.01	<0.01	<0.01	<0.05	<0.01
range: −29.9– −18.4	0.36	0.36	0.38	0.28	0.36
TC (%)				<0.05	
range: 0.1–45.4				−0.26	
TN (%)					
range: 0.1–2.3					
C/N				<0.05	
range: 2.3–44.2				−0.24	
H^+ (cmolc kg^{-1})				<0.05	
range: 0–61.3				−0.24	
K^+ (cmolc kg^{-1})					
range: 0.1–2.0					
Na^+ (cmolc kg^{-1})	<0.01	<0.01	<0.01	<0.01	<0.01
range: 0.01–0.89	0.33	0.35	0.36	0.37	0.33
Mn^{2+} (cmolc kg^{-1})					
range: 0.01–0.7					
Ca^{2+} (cmolc kg^{-1})	<0.01	<0.01	<0.01	<0.01	<0.01
range: 0.1–20.9	0.33	0.33	0.34	0.37	0.33
Mg^{2+} (cmolc kg^{-1})	<0.05	<0.05	<0.01	<0.01	<0.05
range: 0.1–6.6	0.30	0.26	0.30	0.33	0.30
Al^{3+} (cmolc kg^{-1})					
range: 0.0–3.2					
Fe^{3+} (cmolc kg^{-1})					
range: 0.0–0.3					
CEC	<0.05				<0.05
range: 2–78	0.23				0.23
Σbases	<0.01	<0.01	<0.01	<0.01	<0.01
range: 1–48	0.33	0.32	0.34	0.37	0.33
Σmetals					
range: 0.01–10					
Basesaturation (%)		<0.01	<0.05	<0.001	
range: 3–100		0.34	0.26	0.46	

they are often below detection limit. To allow the calculation of the ratios, the fractional abundance of lipids that are present below detection limit have been replaced by a random number between 0.0001 and 0.0002. For all calculations, R (version 4.2.2, R Core Team, 2021) and the package vegan (Oksanen et al., 2022) were used.

3. Results and discussion

3.1. Comparing variation in soil chemistry and temperature with global variability

The soil chemistry variability of the soils under study (n = 74), represents the lower range of soil pH present on a global scale (pH < 7; Slessarev et al., 2016). Especially the Indonesian soils can be characterized by very low pH values (pH < 3), and high amounts of soil carbon and free acidity (Supp. Fig. 3). As expected, low pH soils (3 < pH < 4) show increased concentrations of exchangeable Al^{3+} and Fe^{3+} (typically Tanzania and Indonesia SG soils; for Al^{3+} see Supp. Fig. 3) while higher pH soils (4 < pH < 7) show increased amounts of exchangeable bases (typically soils from the Indonesia TC, and China transect, for Ca^{2+} see Supp. Fig. 3). The Air MATs extracted from CHELSA encompass a large range, reflecting the different climate zones and elevations covered in Austria (0.3–6.1 ℃), Bolivia (4.6–20.3 ℃), China (3.2–12.0 ℃), Indonesia (10.8–26.4 ℃) and Tanzania (8.1–22.9 ℃). As expected, Air MAT correlates with mean Air GST (r = 0.94, p < 0.001; Table 1), Soil MAT (r = 0.98, p < 0.001) and Soil Mean Summer Temperature (Soil MST, r = 0.84, p < 0.001). In addition, mean monthly precipitation and actual evaporation correlate with Air MAT (r = 0.58 and 0.91, respectively, p < 0.001), resulting in a weak trend between Air MAT and the P/E ratio (r = -0.27, p < 0.05; Table 1).

Linear correlations allow determination of which climate and soil chemistry parameters covary with Air MAT, prior to interpreting correlations with individual GDGTs. Soil TC (0.1–45.5 %), TN (0.1–2.3 %), derived C/N ratios (w/w: 2.3–44.2) and bulk $\delta^{15}N$ (-1.5–8.5 ‰) show a large variability that shows no or weak correlations with temperature parameters (Table 1). Bulk $\delta^{13}C$ (-29.9 – −18.4 ‰), increases in this dataset with temperature (0.28 < r < 0.38, p < 0.05). Furthermore, soil pH generally increases with temperature parameters (0.23 < r < 0.44, p < 0.05), as well as the exchangeable soil cations Na^{+}, Ca^{2+} and Mg^{2+} (0.26 < r < 0.37, p < 0.05; Supp. Fig. 3 for Soil MST). This results in a statistically significant correlation between the soil chemical parameter Σbases and temperatures (0.32 < r < 0.37, p < 0.01; Table 1). These interdependencies will be considered when discussing the climate and soil chemistry drivers on GDGT concentrations. However, the interdependencies are unique to the mountain transects under study, and should not be extrapolated to low-altitude soils on a global scale, as soils in low-relief tropical landscapes generally have a lower pH and concentration of exchangeable cations, compared to mid- and high-latitude soils (Slessarev et al., 2016). As vegetation and soil granulometry are not included as parameters in this dataset, their proposed effect on soil GDGTs (e.g., Liang et al., 2019) cannot be tested. However, large scale changes in vegetation type and amount are captured indirectly by $\delta^{13}C$, C/N and TOC values.

3.2. Influence of soil chemistry and temperature on brGDGT concentrations and proposed mechanisms

All 15 brGDGTs are encountered in the soils (Supp. Table 1), where brGDGT Ia is the most abundant compound (fractional abundance, 28–89 %). 5-methyl brGDGTs IIa, IIb, IIc, IIIa, IIIb, IIIc (1.5–56 %) are generally present in higher abundance than their 6-methyl counterparts IIa', IIb', IIc', IIIa', IIIb', IIIc' (0.3–29 %). The summed concentration of brGDGTs (only quantified in the 36 IAEA soils samples) varies between 160 and 5000 ng g $soil^{-1}$. The concentration of individual brGDGTs, normalized per g soil, is governed by one of three sets of drivers (Fig. 1A, Supp. Table 2): (i) brGDGTs Ia, Ib, Ic, IIa, IIb, IIc and IIc' increase with TN, TC content and free acidity, (ii) brGDGTs IIa and especially IIIa and IIIc decrease with temperature, while (iii) the concentrations of brGDGTs Ib, IIb, IIa' and IIb' increase with the concentration of exchangeable cations (summarized as CEC and Σbases). After

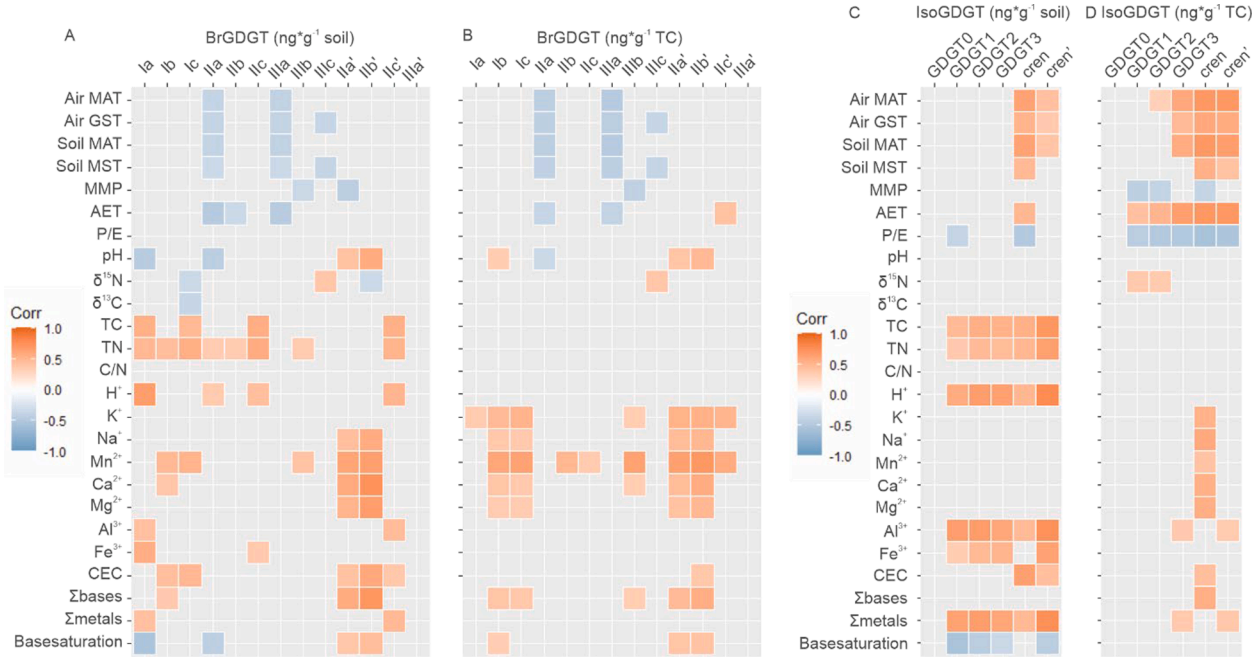

Fig. 1. Visual representation of the significant (p > 0.05) linear correlations between brGDGT (A-B) and isoGDGT (C-D) concentrations and environmental variables, where colors indicate the value of the Pearson r-value. Concentrations are normalized either per g soil (A, C) or per g C (B, D). Environmental variables are Air MAT = air mean annual temperature, Air GST = air growing season temperature, Soil MAT = soil mean annual temperature, Soil MST = soil mean summer temperature, MMP = mean monthly precipitation, AET = actual evapotranspiration, P/E = precipitation/evaporation ratio, soil pH, $\delta^{15}N$ and $\delta^{13}C$ on bulk soils, total carbon (TC), total nitrogen (TN), ratio of TC over TN (C/N), free acidity (H^{+}), exchangeable cations K^{+}, Na^{+}, Mn^{2+}, Ca^{2+}, Mg^{2+}, Al^{3+} and Fe^{3+}, and derived ratios Cation Exchange Capacity (CEC), sum of bases and metals (Σbases and Σmetals, respectively) and base saturation (Basesaturation).

normalization on TC, brGDGT concentrations still respond to two of these drivers, i.e., temperature and exchangeable cations, as the first set (TN, TC and free acidity) strongly correlates with TC. Importantly, the same compounds respond to temperature and exchangeable cations when evaluating either concentration per gram soil, or TC-normalized concentration, although the latter generally show slightly higher correlation coefficients (Supp. Table 2). First, the total and TC-normalized concentrations changes are discussed to identify potential mechanisms (specifically, bacterial community change or membrane adaptation) that drive the production of brGDGTs. Here, the shared increase in concentration per g soil of tetramethylated and 5-methyl penta- and hexamethylated brGDGTs with TN content (Fig. 1A) can be explained if all of these compounds are produced by the same bacterial species (or group of bacteria), that can potentially be active in the N cycle, as microbial biomass active in organic N mineralization has been observed to increase with N content in several soil grain sizes (Hassink, 1995). Given that the capacity to depolymerize organic N is especially strongly expressed in the phylum Acidobacteria (Nguyen et al., 2019), which has been proposed to host the producers of brGDGTs, we suggest that the producer(s) of brGDGTs function(s) as generalists (i.e., mineralizing organic N). Superimposed on the observed increase with TN, the concentration of the major brGDGT Ia shows an increase with free acidity. A previous study has linked this to a change in the bacterial community composition (Halffman et al., 2022), where amidst several clades an increase in Acidobacteria subgroups 1 and 3 is observed. The concentration increase of brGDGT Ia in soils with free acidity potentially reflects a contribution of an additional bacterial producer in these low pH soils as well.

Based on our data, collected along 6 elevation transects, a direct impact of temperature on the concentration of brGDGT Ia is thus not supported (Fig. 1A; Supp. Table 2). Specifically, we found no link between the concentration of brGDGT Ia with either temperature parameters or the P/E ratio, indicating that free acidity, or another, untargeted soil parameter, is the main driver of the production of brGDGT Ia in the soils along the elevation transects. Instead, brGDGT IIa, IIIa and IIIc show a temperature response, decreasing in concentration in warmer soils (Fig. 1A-B). The concentration of brGDGT IIa seems to be influenced both by pH and temperature (high values only in acid soils, and low values generally in warm alkaline soils), while IIIa only shows a temperature effect (Fig. 1A-B). Culture studies have shown the increase in fractional abundance of brGDGTs IIa and IIIa in cold growth environments (Chen et al., 2022; Halamka et al., 2023), which indicates that a membrane adaptation potentially explains the variation in brGDGTs IIa and IIIa. However, as temperature-driven concentration changes of individual brGDGTs in cultures have not been reported, it is not a conclusive explanation for the observed concentration changes in soils yet.

The concentration changes of two other groups of compounds, pentamethylated 6-methyl brGDGTs IIa', IIb' and IIc', as well as the cyclopentane-containing brGDGTs (Ib, Ic, IIb, IIc, IIIb) show subtle differences that can be related to a change in bacterial producer (Fig. 1A-B, Supp. Table 2). Specifically, 6-methyl brGDGTs (IIa', IIb', IIc') show strong correlations with cation concentrations (Fig. 1A-B), while cyclopentane-containing tetramethylated and 5-methyl GDGTs (Ib, Ic, IIb, IIc, IIIc), correlate mainly with TN, similar to the major brGDGTs Ia and IIa. Their shared correlation with cations becomes more apparent after TC-normalization (Fig. 1A-B). A separate bacterial source for 6-methyl brGDGTs is supported by work with pure cultures (Sinninghe Damsté et al., 2018), where 6-methyl brGDGT precursors are so far encountered exclusively in Acidobacteria subgroup (SG) 6. In addition, environmental studies have linked 6-methyl GDGT concentrations to increases in the relative abundance of Acidobacteria SG 4 and 6 (De Jonge et al., 2021). Although GDGT-based ratios based on these compounds are calibrated against soil pH on the global scale (De Jonge et al., 2014a; Xiao et al., 2015), soil pH shows a weaker correlation with the concentration of these compounds compared to Mn^{2+} and Ca^{2+}. In

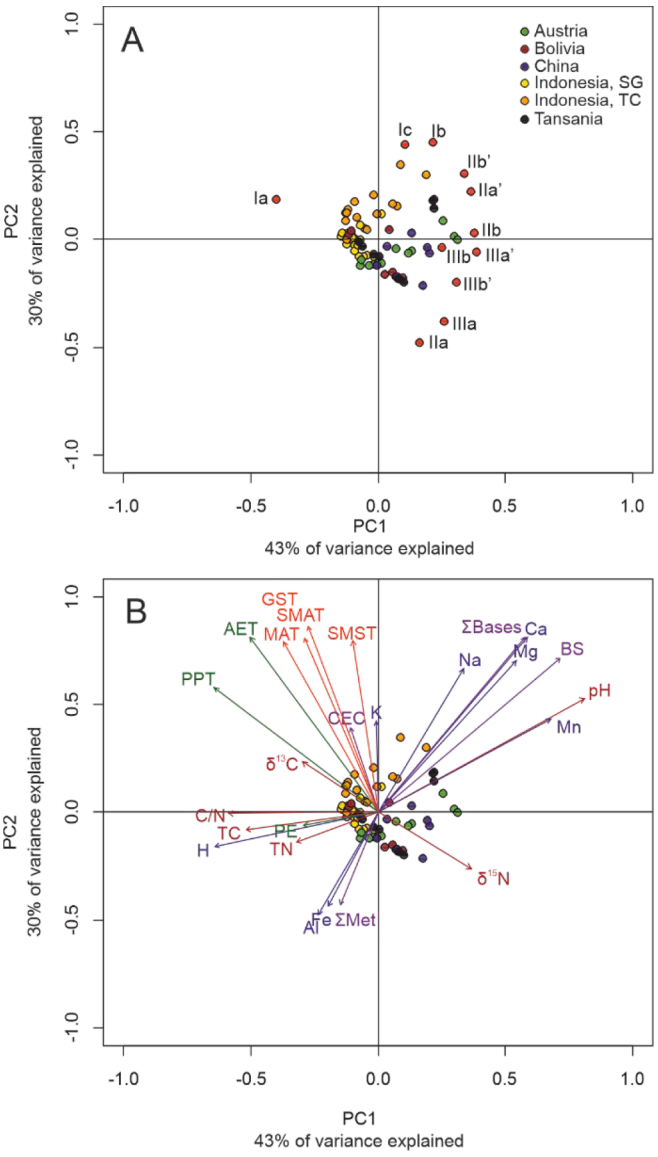

Fig. 2. PCA based on standardized fractional abundances of brGDGTs. Environmental variables (plotted *a posteriori*) are Air MAT = air mean annual temperature, Air GST = air growing season temperature, Soil MAT = soil mean annual temperature, Soil MST = soil mean summer temperature, AET = actual evapotranspiration, MMP = mean monthly precipitation, PE = precipitation/evaporation ratio, total carbon (TC), total nitrogen (TN), $\delta^{13}C$ and $\delta^{15}N$ on bulk soils, free acidity (H^+), exchangeable cations K^+, Na^+, Mn^{2+}, Ca^{2+}, Mg^{2+}, Al^{3+} and Fe^{3+}, and derived ratios Cation Exchange Capacity (CEC), base saturation (BS) and sum of bases and metals (Σbases and Σmetals, respectively).

natural settings, a direct response of 6-methyl brGDGTs to increasing concentration of exchangeable Ca^{2+} has been observed by Halffman et al. (2022). Similar to their interpretation, we propose that an increase in Ca^{2+}, a known driver of increases in Acidobacteria SG 4, 6 and 7 (in addition to Mg^{2+}; Kielak et al., 2016), caused the increased abundance of 6-methyl brGDGTs IIa', IIb' and IIc'. Mn^{2+}, a redox-sensitive cation, is not identified as a driver of GDGT distributions along a single altitudinal transect by Halffman et al. (2022), nor is it known as a strong driver of bacterial community changes (Navarrete et al., 2013). Still, based on the observed correlations it should be considered as a possible driver for the production of 6-methyl and cyclopentane-containing brGDGTs ($0.35 < r < 0.70$, $p < 0.05$; Fig. 1A-B, Supp. Table 2B) in soils.

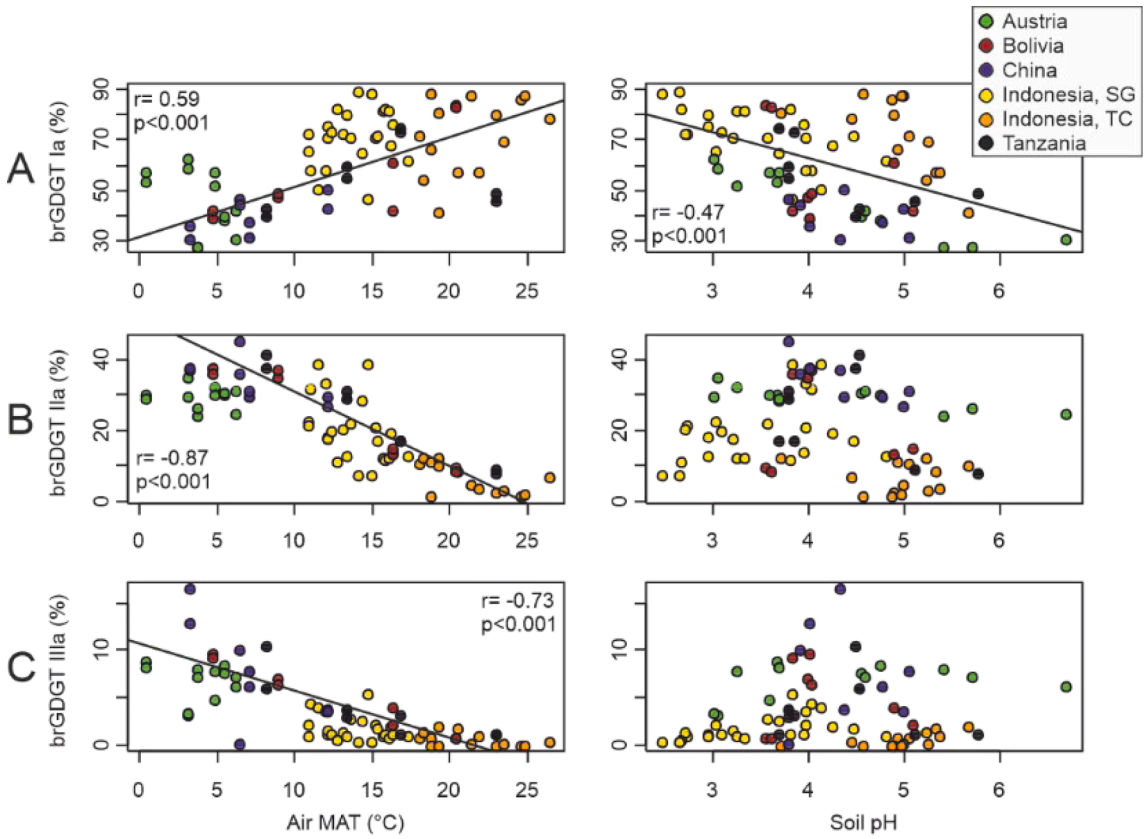

Fig. 3. Fractional abundance (%) of A) brGDGT Ia, B) IIa and C) IIIa. Plotted vs Air MAT (left panels) and soil pH (measured in 1 M KCl; right panels). The black line plots the regression line for significant correlations (r-value reported).

3.3. Influence of soil pH and temperature on brGDGT relative distributions and MBT'$_{5ME}$, CBT', IR, and DC' proxies

The environmental distribution of the fractional abundances of brGDGTs ($n_{samples} = 74$) reflects the impact of both temperature and soil chemistry (Supp. Table 3). To investigate the combined drivers on brGDGT fractional abundances, a PCA based on the standardized fractional abundance of 11 brGDGTs that are consistently present above detection limit (excluding compounds IIc, IIc', IIIc and IIIc') was performed (Fig. 2). An RDA is used to identify the drivers that explain significant amount of variation in GDGT fractional abundances (Supp. Fig. 4A). For brGDGTs, 69 % of the variance can be explained by changes in Air MAT, Air GST, Soil MAT, $\delta^{13}C$, Mg^{2+}, pH and K^{+} (Supp. Fig. 4C; Supp. Table 6), which dominantly reflect those environmental variables that are driving the concentration changes (Fig. 1A-B).

MBT'$_{5ME}$ values [Eq. 1] vary between 0.38 and 0.99, which corresponds to 72 % of the full range encountered on a global scale (Dearing Crampton-Flood et al., 2020). The different impact of Air MAT and soil pH on the fractional abundance of the three most abundant brGDGTs that determine variation in the MBT'$_{5ME}$, i.e., brGDGT Ia, IIa, IIIa, has been visualized in Fig. 3. Here, panel A shows the impact of both soil pH and Air MAT on brGDGT Ia ($|r|>0.47$, $p < 0.001$), while panels B and C show the temperature dependency on brGDGT IIa and IIIa, and no correlation with soil pH. As the concentration of brGDGT Ia does not correlate with temperature, this implies that the fractional abundance of brGDGT Ia (Fig. 3A) only increases with temperature by virtue of decreasing concentrations of the more methylated GDGTs. This is also clear from the PCA, where brGDGT Ia plots opposite brGDGT IIa and IIIa (Fig. 2). Because of the earlier established relationship between brGDGT Ia and free acidity, a correlation between the fractional abundance of brGDGT Ia and pH ($r = -0.47$, Fig. 3A) is observed, which results in high MBT'$_{5ME}$ values in low pH soils (Fig. 4A-B). Specifically, acidic soils with pH < 3.7, generally have a warm to very warm bias in reconstructed temperature (offset varies between −2.9 to + 10.3, average = +4.2 ℃, n = 23, Fig. 4B). The unique effect of temperature on the fractional abundance of brGDGT IIIa was previously shown across a hydrothermal warming gradient in soils (De Jonge et al., 2019), and along an altitudinal transect (Véquaud et al., 2021). Furthermore, the dependency of fractional abundance of brGDGT Ia with soil pH (pH range 2.5–7.6) and free acidity (range 0–61 cmolc kg^{-1}) remains valid when previously published data (Halffman et al., 2019 and Véquaud et al., 2021) are included (Supp. Fig. 5). Importantly, this pH effect is fundamentally different from the impact of 6-methyl brGDGTs as described in De Jonge et al. (2021) who showed that the concentration increase in 6-methyl brGDGTs in high pH soils (pH > 6.3) results in a decrease in the relative abundances of Ia, IIa and IIIa. This impacts the MBT'$_{5ME}$ due to a change in the relative abundances of brGDGT Ia, IIa and IIIa between high and low pH soils. De Jonge et al. (2021) proposed that this change in relationship with pH occurs at around 6.3 and is potentially caused by the change in microbial composition that occurs between alkaline and acid soils. Thus, while across larger pH gradients, pH dependent changes in the fractional abundance of brGDGT IIa and IIIa have been observed (De Jonge et al., 2021), within low pH soils this effect is expected to be absent, which is confirmed here, as there is no correlation between the fractional abundance of IIa and IIIa and pH (Fig. 3B–C, Supp. Table 3). Instead, it is the correlation between Ia and pH that results in a consistent overestimation of MBT'$_{5ME}$ values in soils with a low pH. Although the MBT'$_{5ME}$ was introduced to remove the effect of alkalinity-promoted 6-methyl brGDGTs (De Jonge et al., 2014a), a pH dependency thus still remains in low pH soils.

Still, a good correlation of the MBT'$_{5ME}$ index with Air MAT is observed ($r = 0.85$, $p < 0.001$, RSME of reconstructed temperature = 2.7 ℃, Fig. 4A), which is similar to the correlation with Air GST ($r = 0.86$, $p < 0.001$) and Soil MAT ($r = 0.84$, $p < 0.001$) [Table 2]. The correlation is

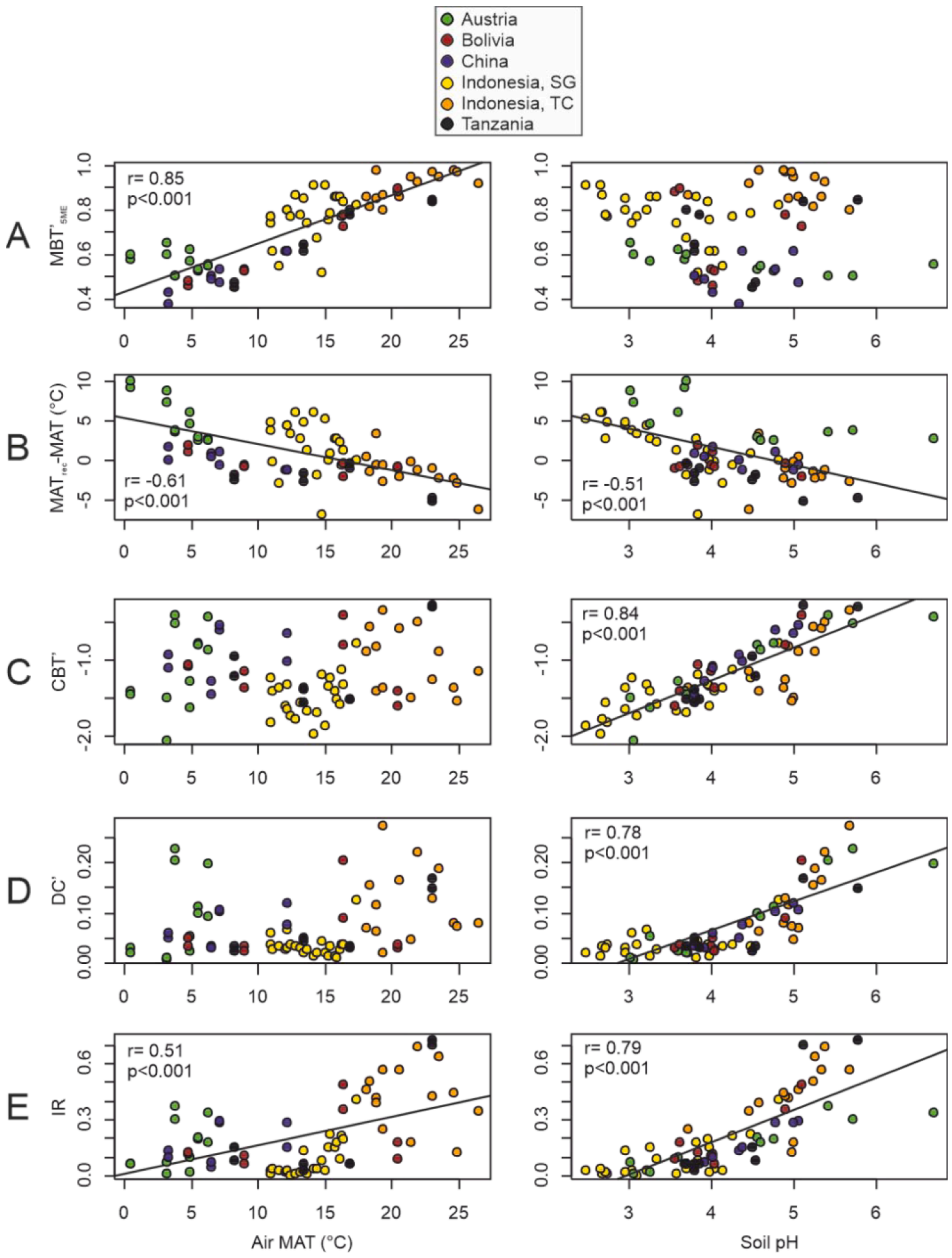

Fig. 4. BrGDGT ratio values plotted against Air MAT (air mean annual temperature; left panels) and pH (measured in 1 M KCl; right panels). A) MBT'$_{5ME}$ values, B) offset between measured Air MAT values and reconstructed temperatures (based on De Jonge et al., (2014a) MBT'$_{5ME}$ calibration [MATrec = -8.57 + 31.45*MBT'$_{5ME}$]), C) CBT' values, D) DC' values, E) IR values. The black line plots the regression line for significant correlations (r-value reported).

not improved by using alternative GDGT-based ratios. For instance, Raberg et al. (2021) proposed to use methylation indices, calculated separately for only the compounds with 0, 1 or 2 cyclopentane groups, as temperature proxies instead of the MBT'$_{5ME}$. Although the fIa$_{Meth}$, fIb$_{Meth}$ and fIc$_{Meth}$ [Eq. 5] all correlate with Air MAT ($r = 0.85$, $r = 0.70$, $r = 0.62$, respectively, $p < 0.001$, Table 2), fIb$_{Meth}$ and fIc$_{Meth}$ also show correlations with exchangeable cations, that are not present in the MBT'$_{5ME}$ and fIa$_{Meth}$, indicating a confounding effect of soil chemistry on the former ratios (Table 2).To improve the accuracy of the MBT'$_{5ME}$ ratio based on this well understood dataset, we test the performance of two correction factors to the global calibration using the MBT'$_{5ME}$ proxy. Firstly, we test a correction for the impact of pH on the MBT'$_{5ME}$ by establishing a multiple linear regression that includes both the MBT'$_{5ME}$ and a GDGT-based pH proxy, the same approach that was used for the MBT' and CBT model (Weijers et al., 2007; Peterse et al., 2012). This calibration allows to correct mathematically for an offset in the reconstructed temperature values. In this dataset, three previously established ratios (IR, CBT' and DC') show a strong correlation with soil pH ($0.78 < r < 0.84$, $p < 0.001$, Table 2). Including IR ratio values in a multiple linear regression results in a decrease in the RSME from 3.4 ℃ ($r = 0.85$) to 3.1 ℃ ($r = 0.88$) on the relationship of brGDGTs with temperature [Calibration B]. Similar attempts using CBT' or DC' instead of IR do not further improve the performance of the model, so only the variant with the IR is discussed here.

Air MAT = -11.21 + 33.58*MBT'$_{5ME}$ [Calibration A, RSME = 3.4 ℃, $r = 0.85$, $n = 74$]

Air MAT = -10.50 + 30.15*MBT'$_{5ME}$ + 8.44*IR [Calibration B, RSME = 3.1 ℃, $r = 0.88$, $n = 74$]

While the pH correction removes the correlation between the residual and pH (Fig. 4B, Supp. Fig. 6B) and improves the accuracy in the

Table 2
Correlation between environmental variables and selected GDGT-based ratios MBT'$_{5ME}$, CBT', IR, DC', fIa$_{meth}$, fIb$_{meth}$, fIc$_{meth}$, TEX$_{86}$, f[CREN'], BIT, Ri/b [Eq. 1–9].

	MBT'$_{5ME}$	CBT'	IR	DC'	fIa$_{meth}$	fIb$_{meth}$	fIc$_{meth}$	TEX$_{86}$	f[CREN']	BIT	Ri/b
Air MAT (°C)	<0.001		<0.001		**<0.001**	<0.001	<0.001	<0.001		<0.05	
range: 0.3–26.4	0.85		0.51		**0.85**	0.70	0.62	0.44		−0.30	
Air GST (°C)	**<0.001**		<0.001	<0.01	<0.001	<0.001	<0.001	<0.001		p < 0.05	
range: 5.0–27.0	**0.86**		0.59	0.32	0.84	0.71	0.66	0.46		−0.27	
Soil MAT (0–5 cm, °C)	<0.001		<0.001	<0.05	<0.001	<0.001	<0.001	<0.001		<0.01	
range: 1.0–25.0	0.84		0.60	0.28	0.83	0.66	0.59	0.47		−0.36	
Soil MST (0–5 cm, °C)	<0.001	<0.05	<0.001	<0.001	<0.001	<0.001	<0.001	**<0.001**		<0.001	<0.05
range: 6.0–25.3	0.71	0.28	0.69	0.43	0.70	0.56	0.54	**0.49**		−0.42	0.27
MMP (mm/month)	<0.001	<0.05			<0.001	<0.001	**<0.001**		<0.01	p < 0.01	<0.001
range: 60–326	0.68	−0.27			0.68	0.74	**0.70**		−0.38	0.32	−0.45
AET (mm/month)	<0.001		<0.001		<0.001	**<0.001**	<0.001	<0.01			
range: 32–113	0.82		0.41		0.82	**0.77**	0.64	0.33			
P/E		<0.01	<0.05					<0.01	<0.01	<0.001	**<0.001**
range: 1.1–4.3		−0.32	−0.24					−0.32	−0.35	0.45	**−0.55**
Soil pH		**<0.001**	**<0.001**	**<0.001**				<0.01		<0.01	<0.01
range: 2.5–6.7		**0.84**	**0.79**	**0.78**				0.34		−0.32	0.35
$\delta^{15}N$ (‰)	<0.01				<0.01	<0.001	<0.001		<0.05	<0.01	<0.001
range: −1.5–8.5	−0.31				−0.30	−0.44	−0.45		0.27	−0.31	0.50
$\delta^{13}C$ (‰)	<0.01				<0.01	<0.05	<0.05		<0.05		
range: −29.9– −18.4	0.35				0.35	0.28	0.29		−0.31		
TC (%)		<0.001	<0.001	<0.001		<0.01	<0.05			<0.05	<0.01
range: 0.1–45.4		−0.50	−0.46	−0.38		0.32	0.30			0.27	−0.32
TN (%)		<0.01	<0.001	<0.01						<0.05	<0.05
range: 0.1–2.3		−0.35	−0.41	0.30						0.23	−0.24
C/N	<0.05	<0.001	<0.01	<0.01	<0.05	<0.01	<0.01	<0.01	<0.05	<0.05	<0.001
range: 2.3–44.2	0.25	−0.50	−0.34	−0.35	0.27	0.36	0.33	−0.38	−0.32	0.27	−0.39
H^+ (cmolc kg^{-1})		<0.001	<0.001	<0.001							
range: 0–61.3		−0.57	−0.49	−0.41							
K^+ (cmolc kg^{-1})	<0.05				<0.05		<0.05			<0.05	
range: 0.1–2.0	0.24				0.24		0.25			−0.24	
Na^+ (cmolc kg^{-1})	<0.05	<0.001	<0.001	<0.001				<0.05		<0.05	
range: 0.01–0.89	0.24	0.46	0.59	0.42				0.25		−0.28	
Mn^{2+} (cmolc kg^{-1})		<0.001	<0.001	<0.001				<0.05			
range: 0.01–0.7		0.57	0.46	0.50				0.24			
Ca^{2+} (cmolc kg^{-1})		<0.001	<0.001	<0.001			<0.01			<0.001	
range: 0.1–20.9		0.61	0.67	0.62			0.36			−0.36	
Mg^{2+} (cmolc kg^{-1})		<0.001	<0.001	<0.001			<0.01			**<0.001**	
range: 0.1–6.6		0.54	0.58	0.48			0.34			**−0.48**	
Al^{3+} (cmolc kg^{-1})		<0.05	<0.01	<0.01		<0.05	<0.05		<0.001		
range: 0.0–3.2		−0.27	−0.33	−0.34		−0.26	−0.29		0.65		
Fe^{3+} (cmolc kg^{-1})		<0.01	<0.001	<0.05		<0.01	<0.05		<0.001		
range: 0.0–0.3		−0.35	−0.39	−0.29		−0.36	−0.25		0.63		
CEC	<0.05				<0.05	<0.05	<0.01				
range: 2–78	0.28				0.27	0.29	0.37				
Σbases		<0.001	<0.001	<0.001			<0.01			<0.001	
range: 1–48		0.60	0.67	0.61			0.37			−0.40	
Σmetals			<0.05	<0.05		<0.05	<0.05		**<0.001**		
range: 0.01–10			−0.28	−0.28		−0.28	−0.28		**0.67**		
Basesaturation (%)		<0.001	<0.001	<0.001				<0.01		<0.05	
range: 3–100		0.71	0.73	0.71				0.29		−0.29	

dataset for low pH soils, the reconstructed temperatures in Austria are still overestimated (Supp. Fig. 6B). In addition, the calibration with pH correction performs worse on the global scale (Calibration B: RSME of 7.2 ℃, r = 0.70) compared to the application of the MBT'$_{5ME}$ calibration without a pH correction (Calibration A: RSME of 5.7 ℃, r = 0.79). This indicates that the environmental conditions in our elevation transects are not directly comparable to the variability in the global soil dataset, possibly due to the narrow range of soil pH in this dataset (2.5–6.7).

A next approach in aligning MBT'$_{5ME}$ values and temperature is to exclude unfavorable growth conditions for heterotrophic bacteria, i.e., when the ground is frozen and dry (Nikrad et al., 2016). Following the approach of Dearing-Crampton Flood et al. (2020) and Naafs et al. (2017), we thus calibrate a model that reflects Air GST. Calibrating the MBT'$_{5ME}$ with GST, results in a slightly improved fit when compared to MAT, reducing the RSME to 2.7 ℃, r = 0.86 [Calibration C].

Air GST = -4.56 + 26.28* MBT'$_{5ME}$ [Calibration C, RSME = 2.7 ℃, r = 0.86, n = 74]

As the low pH Austrian soils, that showed a large offset with reconstructed temperatures (Fig. 4B), are frozen part of the year, they now fit the general trend much better (Supp. Fig. 6D). Although correlation with Air GST has resulted in correcting for the high MBT'$_{5ME}$ values in the Austrian soils, the low pH Indonesian SG soils are still offset from the correlation. Since the residuals of this calibration show a strong relationship with pH, the IR can be included again as a correction. This results in a calibration that allows to reconstruct Air GST with a RSME of 2.2 ℃:

Air GST = -3.82 + 22.71 *MBT'$_{5ME}$ + 8.78 *IR [Calibration D, RSME = 2.2 ℃, r = 0.91, n = 74]

Testing the performance of calibrations C and D on a global scale, the Air GST is reconstructed with an RSME of 4.0 ℃ for both (r = 0.79 and 0.72, respectively), compared to RSME of 5.7 ℃ (r = 0.79) for the Calibration A. The fit (r-value) between MBT'$_{5ME}$ and temperature on the global scale is thus not improved by using Air GST temperature. The RSME cannot be compared, as the range in Air GST values (1.7–28.1 °C),

and thus the associated RSME, is smaller compared to the range in Air MAT values (-17.7–28.5 °C) used in the original calibration. Evaluating the performance of calibrations A-D, and knowing that pH is a driving factor of MBT'$_{5ME}$ offsets in this dataset (Fig. 4B), the IR-based pH correction is a valid approach to improve the accuracy in the elevation transects (Calibrations B and D). Although Air GST does not show a stronger correlation with GDGT concentrations compared to Air MAT, employing a calibration against Air GST improves the accuracy of the calibration. However, this improvement is based dominantly on the low pH soils that are partly present at a location where soils are frozen part of the year (Austria). Hence, the improvement of the calibration using GST should thus in part be attributed to the pH effect. The best understood and mechanistically supported correction is thus applied in Calibration B.

Finally, we employ a statistical approach to further improve the description of the brGDGT-temperature relationship in the elevation transects (c.f. De Jonge et al., 2014a). The following ratio was found to correlate best with Air GST ($r = 0.90$, RSME = 2.2 ℃, $p < 0.001$; Supp. Table 3), in addition showing a good correlation with Air MAT ($r = 0.86$, RSME = 3.3 ℃, $p < 0.001$; Supp. Table 3):

(IIIa + IIIb + IIb'+ Ia + Ib)/(IIIa + IIIa'+ IIIc + IIa + IIb + Ia + Ic)(Eq. 10)

The accuracy of this correlation and associated calibration (Supp. Table 4) is similar to Calibration B, with a slightly increased RSME. Temperature-dependent variation is caused by the introduction of brGDGT IIa in the denominator, a compound that decreases in concentration with temperature. On the other hand, several compounds that are driven by pH appear both in the numerator and denominator, and the physical basis of the ratio is therefore not yet clear. Looking at the fractional abundances in the PCA, the incorporation of the compounds IIa and IIIa' in the denominator, and Ib and IIb' in the nominator, all compounds with high loading on PC2 (Fig. 2), match their incorporation in the temperature proxy. Ic in the denominator on the other hand, is unexpected, as this compound increases in relative abundance with temperature. Furthermore, the ratio includes several compounds that are not present in high abundances, which will make application in geological archives with low GDGT concentration problematic. As such, for future studies we recommend to use the MBT'$_{5ME}$, rather than Eq. 10, for temperature reconstructions. In low pH soils ($pH < 6.7$), Calibration B can be applied.

3.4. brGDGT ratios to constrain soil chemistry changes

To increase the reliability of the MBT'$_{5ME}$ as a proxy for soil temperature, contemporary changes in soil chemistry need to be constrained as part of the past environmental reconstruction. For changes in soil pH, the CBT', IR and DC' can be applied. The CBT' ratio ranges between −2.0 and −0.3 (Supp. Table 1) and is driven both by the 6-methyl brGDGTs and cyclopentane-containing brGDGT Ic [Eq. 2]. The IR (0.01 – 0.73; Supp. Table 1) captures only variation in 6-methyl brGDGTs [Eq. 3], while the DC' (0.01 – 0.28; Supp. Table 1) captures the variation in cyclopentane-containing compounds Ib, IIb and IIb' [Eq. 4]. The DC' and IR correlate significantly (Supp. Fig. 7) and all three ratios show the strongest correlation with soil pH ($0.78 < r < 0.84$, $p < 0.001$, Table 2, Fig. 4C–E), although exchangeable bases are interpreted to be the environmental driver of 6-methyl brGDGTs and cyclopentane-containing 5-methyl brGDGTs. In addition, these proxies show a correlation with several temperature parameters (Table 2). Although this indicates a potential confounding effect of temperature, it potentially reflects the correlation between temperature and soil pH on this scale (Table 1).

To develop proxies for exchangeable bases in soils, we build on the observation that exchangeable Ca^{2+} and the Σbases in soils drive the concentrations of certain cyclopentane-containing brGDGTs (Ib, IIa', IIb': Supp. Table 2). The summed fractional abundance of these compounds equals Eq. 11 (Supp. Fig. 8; Supp. Table 4):

(Ib + IIa'+IIb') / (ΣbrGDGTs) [Eq. 11]

Eq. 11 values correlate well with both Σbases ($r = 0.73$, $p < 0.001$) and exchangeable calcium ($r = 0.74$, $p < 0.001$). As this ratio is developed based on soils that cover a large temperature gradient, it can potentially be applied to reconstruct soil Σbases and exchangeable calcium in different climate regimes. An approach where the statistically best correlation is determined, results in a ratio that correlates strongly with both Σbases and exchangeable calcium ($r = 0.81$ and $r = 0.79$, respectively ($p < 0.001$), Supp. Fig. 8; Supp. Table 4):

(Ib + Ic + IIa + IIb'+IIIa + IIIb)/(Ib + Ic + IIa + IIc + IIIa + IIIb + IIIc)[Eq. 12]

This ratio reflects the increase of brGDGTs IIc and IIIc in soils with increased exchangeable bases. Despite the better performance of this ratio, brGDGTs IIc and IIIc are only minor compounds in most soils, which makes this ratio suitable only for archives with sufficient material or sufficiently high brGDGT concentrations.

3.5. Influence of soil chemistry and temperature on isoGDGT concentration, relative abundance and temperature proxies

IsoGDGTs are present at concentrations of 1–1700 ng g^{-1} soil (Supp. Table 1). Except for isoGDGT0, the concentration of all isoGDGTs correlates strongest with free acidity and soil TC (Fig. 1C). In the non-arid soils under study, the isoGDGT1–3, crenarchaeol and cren' generally follow the same concentration changes (Fig. 1C; Supp. Table 5), indicating that they are potentially derived from the same source organisms. As crenarchaeol and cren' are produced exclusively by Thaumarchaeota, we propose that isoGDGT1–3 are also dominantly produced by Thaumarchaeota in the soils under study. This has been identified as an important prerequisite for the application of the TEX_{86} in the marine system, as contribution of non-Thaumarchaeotal isoGDGTs makes the TEX_{86} invalid as a temperature proxy (e.g., Pancost et al., 2001; Zhang et al., 2011; Wang et al., 2017b). Although the dominant producer of minor isoGDGTs in these soils is interpreted to be Thaumarchaeota, the values of the isoGDGT0/cren ratio in these soils vary between 0 and 112, which indicates that the producer of GDGT0 does not produce minor isoGDGTs 1–3. However, in specific soils, variations in the concentration of individual Thaumarchaeotal lipids show a distinct response. Specifically, isoGDGT1 and 2 show the strongest correlation with exchangeable Al^{3+} concentration in soils, and isoGDGT3 and cren' show the strongest correlation with high free acidity (Fig. 1C, Supp. Table 5, Supp. Fig. 9A for isoGDGT2). Although soil Thaumarchaeota are dominantly members from the I.1b lineage, potential additional producers of the Thaumarchaeotal isoGDGTs in high acidity soils (that also have high amounts of exchangeable Al^{3+}) are Thaumarchaeotal group 1.1c, 1.3 or SAGMCG lineages (Lehtovirta-Morley et al., 2011; Tripathi et al., 2013, 2015; Oton et al., 2016). While archaea from subgroups 1.1c and 1.3 are uncultured and have not been subjected to lipid profiling, SAGMCG member *Nitrosotalea devanaterra* has been shown to produce isoGDGTs (Lehtovirta-Morley et al., 2016; Elling et al., 2017). Concentration changes of crenarchaeol, that correlate significantly with MAT, soil CEC and Σbases (shown for Air MAT in Supp. Fig. 9B), can also potentially be related to archaeal community change. In soil mesocosms, the relative contribution of archaeal members from subgroup I.1a and a subset of members from I.1b has been seen to increase with soil temperature (Tourna et al., 2008). A change in archaeal community composition, possibly within subgroup I.1b, thus possibly drives the increase of the temperature-sensitive isoGDGT crenarchaeol.

TC-normalization removes the original correlation with H^+ and Al^{3+}, where TC-normalized concentrations of isoGDGT1, 2 and 3, crenarchaeol and cren' decrease with increasing P/E conditions, reflecting a relative increase in drier soils (Supp. Table 5B, Supp. Fig. 9B). This is

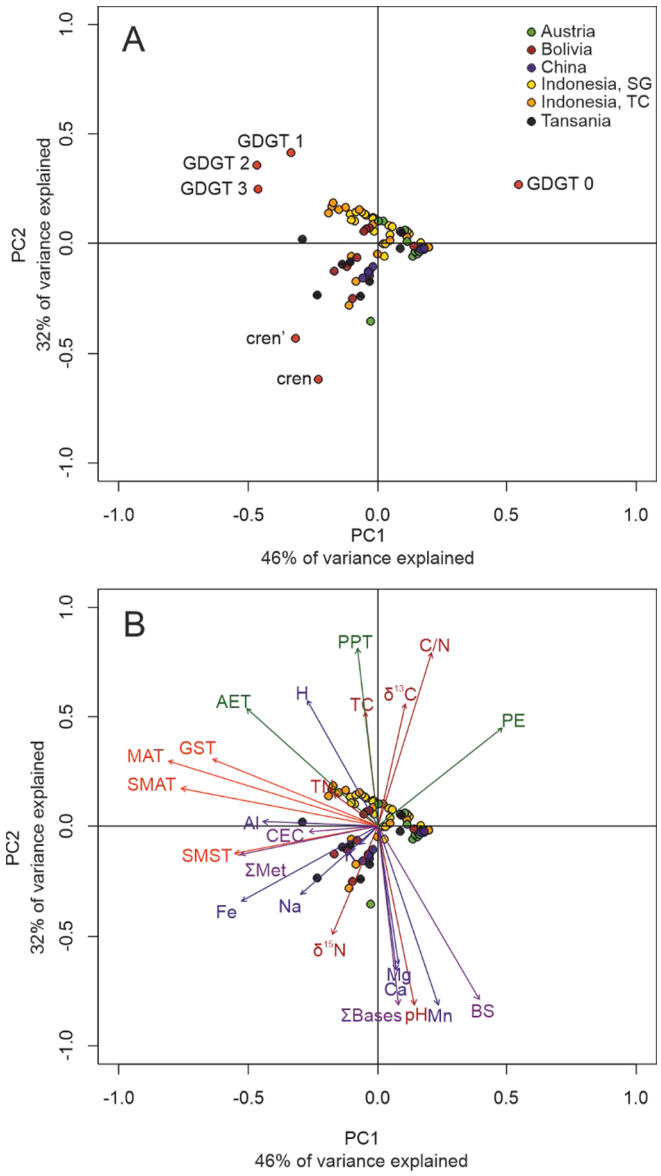

Fig. 5. PCA based on standardized fractional abundances of isoGDGTs. Environmental variables (plotted *a posteriori*) are Air MAT = air mean annual temperature, Air GST = air growing season temperature, Soil MAT = soil mean annual temperature, Soil MST = soil mean summer temperature, AET = actual evapotranspiration, MMP = mean monthly precipitation, PE = precipitation/evaporation ratio (P/E), total carbon (TC), total nitrogen (TN), $\delta^{13}C$ and $\delta^{15}N$ on bulk soils, free acidity (H^+), exchangeable cations K^+, Na^+, Mn^{2+}, Ca^{2+}, Mg^{2+}, Al^{3+} and Fe^{3+}, and derived ratios Cation Exchange Capacity (CEC), base saturation (BS) and sum of bases and metals (Σbases and Σmetals, respectively).

consistent with the largely aerobic niche (Stieglmeier et al., 2014) of ammonia oxidizing ecology of the 1.1b (and SAGMCG) Thaumarchaeotal producer in soils (Pester et al., 2011). Only for crenarchaeol, a better correlation with temperature is observed. As soils with higher concentrations of exchangeable cations are present at higher temperatures along the mountain transects in this dataset, TC-normalized crenarchaeol concentration also correlates positively with exchangeable bases (Fig. 1D, Supp. Table 5B). Contrasting with previous observations by Weijers et al. (2006), who proposed a preferred production of crenarchaeol in soils with pH > 6, crenarchaeol abundance does not correlate with soil pH values in the aerobic soils under study. It also differs from the conclusions from Blewett et al. (2020), who reported an increased concentration of crenarchaeol in wetlands with neutral pore water pH (pH = 6.8) compared to more acid wetlands. Instead, in the pH range of the dataset under study, soil temperature is identified as a potential driver of crenarchaeol concentration in soils, in addition to soil moisture availability.

The PCA of the relative abundances of isoGDGTs in the elevation transects (Fig. 5) illustrates that the fractional abundances of isoGDGTs are indeed dominantly driven by temperature (PC1, 46 % of the variance explained) and soil chemistry parameters (PC2, 32 % of variance explained). The fractional abundances of isoGDGT2 and 3 correlate with Air MAT and the other temperature parameters on PC1, explaining 46 % of the variance, which is at the basis of the temperature dependency of the TEX_{86}. An RDA is performed, revealing that only 36 % of the variance in isoGDGTs can be explained by the parameters available in the dataset. Of these, temperature parameters are the most relevant (Supp. Fig. 4B). A positive correlation between TEX_{86} values in soils and Air MAT has been observed before (e.g., Yang et al., 2016), and a weak but positive correlation is observed here with Air MAT ($r = 0.45$, $p < 0.001$, $r = 0.55$, $p < 0.001$ for $TEX_{86} > 0$; Supp. Fig. 9C), and a slightly stronger correlation with Soil MST ($r = 0.49$, $p < 0.001$, $r = 0.61$, $p < 0.001$ for $TEX_{86} > 0$; Supp. Fig. 9C). As the TEX_{86} includes isoprenoid compounds that decrease in concentration with an increase in P/E (GDGT1 and 2), but also compounds that increase with temperature (GDGT3, cren'), the mechanism of increasing TEX_{86} values in soils might depend both on decreasing soil moisture availability, as well as increasing temperatures. Indeed, when included in a linear model with multiple predictors, P/E is identified as a significantly contributing variable ($p < 0.05$), although it only explains an additional 5 % of variance in the TEX_{86} values (30 % of variance explained increases to 35 % explained). The direction of the effect indicates that the TEX_{86} values at sites with high P/E values (generally low temperatures in this dataset), will be decreased. In addition, the PCA reveals that the correlation between crenarchaeol, cren' and Σbases is independent from the variation in temperature, which is confirmed by the RDA (Supp. Fig. 4D). However, Σbases is not identified as a confounding factor for TEX_{86} values in a multiple predictor linear model.

To improve the correlation between TEX_{86} and temperature in soils, we used a statistical approach and found that the best ratio that correlated with Air MAT and Air GST was defined as follows:

$$(GDGT2 + GDGT3)/GDGT1 \quad \text{[Eq. 13]}$$

The correlation coefficients for this ratio with Air MAT ($r = 0.56$, $p < 0.001$, RSME = 5.4 °C, $n = 68$, Supp. Fig. 9C) and Air GST ($r = 0.57$, $p < 0.001$, RSME = 4.1 °C, $n = 68$) are higher than calculated for the TEX_{86} ($r = 0.45$ and 0.46, for Air MAT and Air GST respectively), but the ratio still performs poorly compared to the brGDGT temperature calibrations ($0.86 > r > 0.71$). Eq. 13 reflects the temperature-dependent increase in TC-normalized concentration of isoGDGT2 and 3, compared to the variation in isoGDGT1, and excludes cren'. Importantly, not all soils in the dataset have quantifiable concentrations of isoGDGT1, 2 and 3 (Eq. 13 cannot be determined for six soils), and application of this ratio might thus be limited to soils with higher concentrations of isoGDGTs.

In addition to the variation explained by temperature and soil moisture availability (P/E), soil chemistry impacts TC-normalized concentrations of isoGDGTs and their distributions, with the TC-normalized concentrations of GDGT3 and cren' still showing a weak correlation with soil exchangeable Al^{3+} (Fig. 1D, Supp. Table 5, Supp. Fig. 9B), indicating that GDGT2, 3 and cren' are produced in soils with exchangeable Al^{3+}. Crenarchaeol on the other hand, remains low in soils with high exchangeable aluminium (Supp. Fig 9B). The mechanism that drives the different behavior of crenarchaeol and its isomer can be elucidated further using the f[CREN'] ratio [Eq. 7]. While the range of f[CREN'] ratio values (0.04–0.42) supports the expected dominance of Thaumarchaeotal group I.1b in these soils (group I.1b cultured members typically have f[CREN'] values between 0.23 and 0.35; Bale et al., 2019) we postulate that the synchronous increase of several isoGDGTs in

response to exchangeable Al^{3+} influence f[CREN'] values in this dataset. A temperature-dependent response of the f[CREN'] ratio as observed in cultures (Bale et al., 2019) is not observed here. The mechanism of the variation with Al^{3+} is only poorly constrained. For instance, the isoGDGT producing SAGMCG lineage has been described to produce low amounts of crenarchaeol and high amounts of GDGT2 and 3 (and also GDGT 4, which has not been measured in this dataset), which can explain a change in GDGT distribution. However, specifically the f[CREN'] value in one cultured SAGMCG member was not high (0.1, Elling et al., 2017), which would need to be explained before invoking a SAGMCG GDGT source. If not caused by a change in archaeal community composition, the f[CREN'] can instead increase as a direct response to soil metal concentrations.

3.6. Developing isoGDGT ratios as soil moisture availability and exchangeable Al^{3+} proxies

Since Al^{3+} or Σmetals, and soil moisture availability impact GDGTs present in the TEX_{86}, we tried to develop ratios that could be used to constrain the variability of these parameters in geological archives. For soil exchangeable Al^{3+} and Σmetals, the statistically best ratio is identical to the f[CREN'] ratio (Baxter et al., 2021). Its values correlate strongly with the concentration of Al^{3+} and Fe^{3+} (Table 2) and Σmetals ($r = 0.67$, $p < 0.001$, r increases to $r = 0.83$, $p < 0.001$ when only samples with f[CREN'] larger than 0 are included, i.e., samples where cren' is above detection limit; Supp. Fig. 9C). Importantly, this dependency is driven mainly by Tanzanian soils, and measuring f[CREN'] values in soils with medium and high amounts of exchangeable metals will be needed to confirm the interpretation of this ratio.

As the P/E value (soil moisture availability) impacts the TC-normalized concentration of all thaumarchaeotal isoGDGTs, it was not possible to develop an isoGDGT ratio that shows a strong correlation with P/E values ($r < 0.40$). However, as mean monthly precipitation (MMP) correlates with crenarchaeol, and does not correlate with GDGT3, a ratio based on isoGDGTs can be developed that tracks MMP ($r = 0.61$, $p < 0.001$, RSME = 47 mm month^{-1}, $n = 69$, Supp. Fig. 8):

$$\text{MMP (mm month}^{-1}) = (\text{GDGT1} + \text{GDGT3})/(\text{GDGT1} + \text{cren}) \quad \text{[Eq. 14]}$$

This ratio is driven by the low concentrations and fractional abundances of crenarchaeol in soils that receive substantial precipitation, while the fractional abundance of GDGT3 is increased in these soils (Supp. Table 3). However, as no ratio could be developed tracing P/E values based on changes in distribution of isoGDGTs, alternative ratios that compare the abundance of brGDGT and isoGDGTs (Ri/b and BIT index) are evaluated next.

3.7. Validating Ri/b and BIT indices as soil moisture proxies

Previous studies showed that the BIT index and Ri/b index decrease and increase respectively with increasing soil aridity, either at a threshold in MAP (<600 mm yr^{-1}; Xie et al., 2012, <750 mm yr^{-1}; Dirghangi et al., 2013), or as a continuous response to decreasing soil water content (SWC; 0–30 % SWC, 2017c,0–60;Wang et al.,% SWC, Dang et al., 2016). In this study, isoGDGTs are present in lower concentration compared to the brGDGTs, resulting in high BIT and low Ri/b values (BIT index = 0.75–0.99 [Eq. 8], Ri/b = 0.00–0.52 [Eq. 9]; Supp. Table 1). The moisture dependency of brGDGT in arid soils observed in an earlier study (i.e., increase with SWC: Menges et al., 2014; Wang et al., 2017c) is not observed in our dataset of non-arid soils under study (MAP > 720–1650 mm yr^{-1}, and a P/E ratio > 1). Instead, TC-normalized concentrations of crenarchaeol, cren', and isoGDGT1–3 increase with decreasing P/E ratio, which matches the observed concentration increase of crenarchaeol (or isoGDGTs) in low MAP soils as observed by Xie et al. (2012) and Yang et al. (2014). In the non-arid soils under study, the correlations between P/E ratio and the BIT index and Ri/b ratio (Table 2, $0.45<|r|<0.55$, Supp. Fig. 8), thus seem to be driven dominantly by isoGDGTs. However, as crenarchaeol, a compound that is also increased in warm soils with high Σbases, is a dominant compound in the BIT index, this proxy correlates both with the P/E ratio, temperature and Σbases (Table 2). The possible impact of temperature on this ratio should thus be considered when interpreting it in paleoclimate records. In our dataset, the Ri/b ratio shows a weak correlation with temperature, and a stronger correlation with the P/E ratio. As it includes all isoGDGTs it is less sensitive to the variation in crenarchaeol. Contingent upon a good understanding of the variation in isoGDGT0, the Ri/b ratio can be a more accurate proxy for soil moisture, within the pH and soil moisture bracket of the soils under study. As such, more research needs to be done before a GDGT-based P/E (as a proxy for soil moisture availability) correction on soil TEX_{86} values can be considered further.

4. Conclusions

The environmental drivers of the concentration and distribution of brGDGTs and isoGDGTs along six elevation gradients located on four continents are identified, to determine the mechanism of temperature dependency and increase the understanding of GDGT based temperature proxies MBT'_{5ME} and TEX_{86}. As the mechanisms described are not unique to soils located on altitudinal gradients, the interpretations are also valid for lowland soils. Although both the MBT'_{5ME} and TEX_{86} show significant correlations with temperature, soil chemistry (free acidity or pH) impacts brGDGT-based MBT'_{5ME} values, and soil moisture availability (approximated here by the P/E ratio) impacts TEX_{86} values. This potentially impacts existing MBT'_{5ME} based temperature reconstructions in non-arid soil profiles where free acidity or pH have changed (pH range between 2.5 and 6.7), or TEX_{86} based temperature reconstructions where soil moisture has varied. To increase confidence in existing and future GDGT-based temperature proxies, changes in soil chemistry should be considered, in parallel with temperature. In addition to traditional pH proxies CBT' and IR that are usually calibrated against pH, novel proxies are developed to reflect exchangeable calcium and Σbases in soils directly. Based on the correlation between exchangeable iron (and Σmetals) and cren', it is proposed to use the f[CREN'] ratio to track this parameter through time. In addition, the Ri/b index is proposed as a ratio for soil moisture availability in non-arid soils. However, further work is required to establish the proposed impact of soil chemistry in low altitude soils, where especially the concentration of exchangeable cations (soil metals like Fe^{3+} and Al^{3+}, soil bases like Ca^{2+} and Mg^{2+}), in addition to the known confounding factors pH and soil moisture content, appear to be a promising target. Following successful application of these proxies in paleosol settings, this should lead to improved reliability of the GDGT-based temperature reconstruction in the terrestrial realm. Ultimately, obtaining a good understanding of the mechanism of temperature dependency and the variability of the confounding factors, is a necessary step in the development of a new generation of models for GDGT-based temperature reconstruction.

Declaration of Competing Interest

The authors declare that they have no known competing financial interests or personal relationships that could have appeared to influence the work reported in this paper.

Data availability

The data used for this publication is included in the editable tables.

Acknowledgments

We acknowledge the insightful comments of two anonymous reviewers and the editorial team that have improved the manuscript. The

authors of this manuscript acknowledge the following funding agencies; SNSF PRIMA Fellowship (PR00P2_179783) to CDJ, Swedish National Science Foundation (VR) grant 2017-04430 to RS, Bolin Center for Climate Research funded field work on Sumatra to PH. Soils from Austria, Bolivia, China and Tanzania are collected through the regional Technical Cooperation Project INT5153, from the International Atomic Energy Agency (IAEA). A NWO-Vidi grant (192.074) was awarded to FP. In addition, we are grateful for assistance in processing samples for analysis on EA-irms (ETH Zurich) by Madalina Jäggi.

Appendix A. Supplementary material

Supplementary data to this article can be found online at https://doi.org/10.1016/j.orggeochem.2023.104706.

References

Abatzoglou, J.T., Dobrowski, S.Z., Parks, S.A., Hegewisch, K.C., 2018. TerraClimate, a high-resolution global dataset of monthly climate and climatic water balance from 1958–2015. Scientific Data 5, 170191.

Anderson, V.J., Shanahan, T.M., Saylor, J.E., Horton, B.K., Mora, A.R., 2014. Sources of local and regional variability in the MBT′/CBT paleotemperature proxy: Insights from a modern elevation transect across the Eastern Cordillera of Colombia. Organic Geochemistry 69, 42–51.

Auguet, J.-C., Barberan, A., Casamayor, E.O., 2010. Global ecological patterns in uncultured Archaea. The ISME Journal 4, 182–190.

Bale, N.J., Palatinszky, M., Rijpstra, W.I.C., Herbold, C.W., Wagner, M., Sinninghe Damsté, J.S., 2019. Membrane lipid composition of the moderately thermophilic ammonia-oxidizing archaeon "Candidatus nitrosotenuis uzonensis" at different growth temperatures. Applied and Environmental Microbiology 85, e01332–e10419.

Bates, S.T., Berg-Lyons, D., Caporaso, J.G., Walters, W.A., Knight, R., Fierer, N., 2011. Examining the global distribution of dominant archaeal populations in soil. The ISME Journal 5, 908–917.

Baxter, A.J., van Bree, L.G.J., Peterse, F., Hopmans, E.C., Villanueva, L., Verschuren, D., Sinninghe Damsté, J.S., 2021. Seasonal and multi-annual variation in the abundance of isoprenoid GDGT membrane lipids and their producers in the water column of a meromictic equatorial crater lake (Lake Chala, East Africa). Quaternary Science Reviews 273, 107263.

Blewett, J., Naafs, B.D.A., Gallego-Sala, A.V., Pancost, R.D., 2020. Effects of temperature and pH on archaeal membrane lipid distributions in freshwater wetlands. Organic Geochemistry 148, 104080.

Chen, Y., Zheng, F., Yang, H., Yang, W., Wu, R., Liu, X., Liang, H., Chen, H., Pei, H., Zhang, C., Pancost, R.D., Zeng, Z., 2022. The production of diverse brGDGTs by an Acidobacterium providing a physiological basis for paleoclimate proxies. Geochimica et Cosmochimica Acta 337, 155–165.

Coffinet, S., Huguet, A., Williamson, D., Fosse, C., Derenne, S., 2014. Potential of GDGTs as a temperature proxy along an altitudinal transect at Mount Rungwe (Tanzania). Organic Geochemistry 68, 82–89.

Coffinet, S., Huguet, A., Pedentchouk, N., Bergonzini, L., Omuombo, C., Williamson, D., Anquetil, C., Jones, M., Majule, A., Wagner, T., Derenne, S., 2017. Evaluation of branched GDGTs and leaf wax n-alkane δ2H as (paleo) environmental proxies in East Africa. Geochimica et Cosmochimica Acta 198, 182–193.

Dearing Crampton-Flood, Emily, Tierney, Jessica E, Peterse, Francien, Kirkels, Frédérique M S A, Sinninghe Damsté, Jaap S, 2019. Global soil and peat branched GDGT compilation dataset.

Dang, X., Yang, H., Naafs, B.D.A., Pancost, R.D., Xie, S., 2016. Evidence of moisture control on the methylation of branched glycerol dialkyl glycerol tetraethers in semi-arid and arid soils. Geochimica et Cosmochimica Acta 189, 24–36.

De Jonge, C., Hopmans, E.C., Zell, C.I., Kim, J.-H., Schouten, S., Sinninghe Damsté, J.S., 2014a. Occurrence and abundance of 6-methyl branched glycerol dialkyl glycerol tetraethers in soils: Implications for palaeoclimate reconstruction. Geochimica et Cosmochimica Acta 141, 97–112.

De Jonge, C., Stadnitskaia, A., Hopmans, E.C., Cherkashov, G., Fedotov, A., Sinninghe Damsté, J.S., 2014b. In situ produced branched glycerol dialkyl glycerol tetraethers in suspended particulate matter from the Yenisei River, Eastern Siberia. Geochimica et Cosmochimica Acta 125, 476–491.

De Jonge, C., Radujković, D., Sigurdsson, B.D., Weedon, J.T., Janssens, I., Peterse, F., 2019. Lipid biomarker temperature proxy responds to abrupt shift in the bacterial community composition in geothermally heated soils. Organic Geochemistry 137, 103897.

De Jonge, C., Kuramae, E.E., Radujković, D., Weedon, J.T., Janssens, I.A., Peterse, F., 2021. The influence of soil chemistry on branched tetraether lipids in mid- and high latitude soils: implications for brGDGT- based paleothermometry. Geochimica et Cosmochimica Acta 310, 95–112.

Dearing Crampton-Flood, E., Tierney, J.E., Peterse, F., Kirkels, F.M.S.A., Sinninghe Damsté, J.S., 2020. BayMBT: A Bayesian calibration model for branched glycerol dialkyl glycerol tetraethers in soils and peats. Geochimica et Cosmochimica Acta 268, 142–159.

Dirghangi, S.S., Pagani, M., Hren, M.T., Tipple, B.J., 2013. Distribution of glycerol dialkyl glycerol tetraethers in soils from two environmental transects in the USA. Organic Geochemistry 59, 49–60.

Duan, Y., Sun, Q., Werne, J.P., Yang, H., Jia, J., Wang, L., Xie, H., Chen, F., 2020. Soil pH Dominates the Distributions of Both 5- and 6-Methyl Branched Tetraethers in Arid Regions. Journal of Geophysical Research. Biogeosciences 125 e2019JG005356.

Duan, Y., Sun, Q., Werne, J.P., Hou, J., Yang, H., Wang, Q., Khormali, F., Xia, D., Chu, G., Chen, F., 2022. General Holocene warming trend in arid Central Asia indicated by soil isoprenoid tetraethers. Global and Planetary Change 215, 103879.

Elling, F.J., Könneke, M., Nicol, G.W., Stieglmeier, M., Bayer, B., Spieck, E., de la Torre, J.R., Becker, K.W., Thomm, M., Prosser, J.I., Herndl, G.J., Schleper, C., Hinrichs, K.-U., 2017. Chemotaxonomic characterisation of the thaumarchaeal lipidome. Environmental Microbiology 19, 2681–2700.

Ernst, N., Peterse, F., Breitenbach, S.F.M., Syiemlieh, H.J., Eglinton, T.I., 2013. Biomarkers record environmental changes along an altitudinal transect in the wettest place on Earth. Organic Geochemistry 60, 93–99.

Guo, J., Ma, T., Liu, N., Zhang, X., Hu, H., Ma, W., Wang, Z., Feng, X., Peterse, F., 2022. Soil pH and aridity influence distributions of branched tetraether lipids in land soils along an aridity transect. Organic Geochemistry 164, 104347.

Halamka, T.A., McFarlin, J.M., Younkin, A.D., Depoy, J., Dildar, N., Kopf, S.H., 2021. Oxygen limitation can trigger the production of branched GDGTs in culture. Geochemical Perspectives Letters 36–39.

Halamka, T.A., Raberg, J.H., McFarlin, J.M., Younkin, A.D., Mulligan, C., Liu, X.-L., Kopf, S.H., 2023. Production of diverse brGDGTs by Acidobacterium Solibacter usitatus in response to temperature, pH, and O2 provides a culturing perspective on brGDGT proxies and biosynthesis. Geobiology 21, 102–118.

Halffman, R., Lembrechts, J., Radujković, D., De Gruyter, J., Nijs, I., De Jonge, C., 2022. Soil chemistry, temperature and bacterial community composition drive brGDGT distributions along a subarctic elevation gradient. Organic Geochemistry 163, 104346.

Hällberg, P., Schenk, S., Jarne-Bueno, G., Schankat, Y., Zhang, Q., Rifai, H., Phua, M., Smittenberg, R.H., 2023. Branched GDGT source shift identification allows improved reconstruction of an 8,000-year warming trend on Sumatra. Organic Geochemistry. https://doi.org/10.1016/j.orggeochem.2023.104702, 104702 (in press.

Hobbins, M.T., Wood, A., McEvoy, D.J., Huntington, J.L., Morton, C., Anderson, M., Hain, C., 2016. The evaporative demand drought index. Part I: linking drought evolution to variations in evaporative demand. Journal of Hydrometeorology 17, 1745–1761.

Hopmans, E.C., Weijers, J.W.H., Schefuß, E., Herfort, L., Sinninghe Damsté, J.S., Schouten, S., 2004. A novel proxy for terrestrial organic matter in sediments based on branched and isoprenoid tetraether lipids. Earth and Planetary Science Letters 224, 107–116.

Hopmans, E.C., Schouten, S., Sinninghe Damsté, J.S., 2016. The effect of improved chromatography on GDGT-based palaeoproxies. Organic Geochemistry 93, 1–6.

Huguet, C., Hopmans, E.C., Febo-Ayala, W., Thompson, D.H., Sinninghe Damsté, J.S., Schouten, S., 2006. An improved method to determine the absolute abundance of glycerol dibiphytanyl glycerol tetraether lipids. Organic Geochemistry 37, 1036–1041.

Inglis, G.N., Collinson, M.E., Riegel, W., Wilde, V., Farnsworth, A., Lunt, D.J., Valdes, P., Robson, B.E., Scott, A.C., Lenz, O.K., Naafs, B.D.A., Pancost, R.D., 2017. Mid-latitude continental temperatures through the early Eocene in western Europe. Earth and Planetary Science Letters 460, 86–96.

Jaeschke, A., Rethemeyer, J., Lappé, M., Schouten, S., Boeckx, P., Schefuß, E., 2018. Influence of land use on distribution of soil n-alkane δD and brGDGTs along an altitudinal transect in Ethiopia: Implications for (paleo)environmental studies. Organic Geochemistry 124, 77–87.

Karger, D.N., Conrad, O., Böhner, J., Kawohl, T., Kreft, H., Soria-Auza, R.W., Zimmermann, N.E., Linder, H.P., Kessler, M., 2017. Climatologies at high resolution for the earth's land surface areas. Scientific Data 4, 170122.

Kielak, A.M., Barreto, C.C., Kowalchuk, G.A., van Veen, J.A., Kuramae, E.E., 2016. The ecology of acidobacteria: moving beyond genes and genomes. Frontiers in Microbiology 7. https://doi.org/10.3389/fmicb.2016.00744.

Kirkels, F.M.S.A., Ponton, C., Galy, V., West, A.J., Feakins, S.J., Peterse, F., 2020. From Andes to amazon: assessing branched tetraether lipids as tracers for soil organic carbon in the madre de dios river system. Journal of Geophysical Research: Biogeosciences 125 e2019JG005270.

Lal, R., 2017. Encyclopedia of Soil Science, 3rd ed. CRC Press, Boca Raton. doi:10.1081/e-ess3.

Lauretano, V., Kennedy-Asser, A.T., Korasidis, V.A., Wallace, M.W., Valdes, P.J., Lunt, D.J., Pancost, R.D., Naafs, B.D.A., 2021. Eocene to oligocene terrestrial southern hemisphere cooling caused by declining pCO2. Nature Geoscience 14, 659–664.

Lehtovirta-Morley, L.E., Stoecker, K., Vilcinskas, A., Prosser, J.I., Nicol, G.W., 2011. Cultivation of an obligate acidophilic ammonia oxidizer from a nitrifying acid soil. Proceedings of the National Academy of Sciences 108, 15892–15897.

Lehtovirta-Morley, L.E., Sayavedra-Soto, L.A., Gallois, N., Schouten, S., Stein, L.Y., Prosser, J.I., Nicol, G.W., 2016. Identifying potential mechanisms enabling acidophily in the ammonia-oxidizing archaeon "candidatus nitrosotalea devanaterra". Applied and Environmental Microbiology 82, 2608–2619.

Leininger, S., Urich, T., Schloter, M., Schwark, L., Qi, J., Nicol, G.W., Prosser, J.I., Schuster, S.C., Schleper, C., 2006. Archaea predominate among ammonia-oxidizing prokaryotes in soils. Nature 442, 806–809.

Lembrechts, J.J., van den Hoogen, J., Aalto, J., Ashcroft, M.B., De Frenne, P., Kemppinen, J., Kopecký, M., Luoto, M., Maclean, I.M.D., Nijs, I., Lenoir, J., 2022. Global maps of soil temperature. Global Change Biology 28, 3110–3144.

Liang, J., Russell, J.M., Xie, H., Lupien, R.L., Si, G., Wang, J., Hou, J., Zhang, G., 2019. Vegetation effects on temperature calibrations of branched glycerol dialkyl glycerol tetraether (brGDGTs) in soils. Organic Geochemistry 127, 1–11.

Liu, W., Wang, H., Zhang, C.L., Liu, Z., He, Y., 2013. Distribution of glycerol dialkyl glycerol tetraether lipids along an altitudinal transect on Mt. Xiangpi, NE Qinghai-Tibetan Plateau. China. Organic Geochemistry 57, 76–83.
Loomis, S.E., Russell, J.M., Sinninghe Damsté, J.S., 2011. Distributions of branched GDGTs in soils and lake sediments from western Uganda: Implications for a lacustrine paleothermometer. Organic Geochemistry 42, 739–751.
Menges, J., Huguet, C., Alcañiz, J.M., Fietz, S., Sachse, D., Rosell-Melé, A., 2014. Influence of water availability in the distributions of branched glycerol dialkyl glycerol tetraether in soils of the Iberian Peninsula. Biogeosciences 11, 2571–2581.
Naafs, B.D.A., Gallego-Sala, A.V., Inglis, G.N., Pancost, R.D., 2017. Refining the global branched glycerol dialkyl glycerol tetraether (brGDGT) soil temperature calibration. Organic Geochemistry 106, 48–56.
Navarrete, A.A., Kuramae, E.E., de Hollander, M., Pijl, A.S., van Veen, J.A., Tsai, S.M., 2013. Acidobacterial community responses to agricultural management of soybean in Amazon forest soils. FEMS Microbiology Ecology 83, 607–621.
Nguyen, T.T.H., Myrold, D.D., Mueller, R.S., 2019. Distributions of Extracellular Peptidases Across Prokaryotic Genomes Reflect Phylogeny and Habitat. Frontiers in Microbiology 10. https://doi.org/10.3389/fmicb.2019.00413.
Nicol, G.W., Leininger, S., Schleper, C., Prosser, J.I., 2008. The influence of soil pH on the diversity, abundance and transcriptional activity of ammonia oxidizing archaea and bacteria. Environmental Microbiology 10, 2966–2978.
Nieto-Moreno, V., Rohrmann, A., van der Meer, M.T.J., Sinninghe Damsté, J.S., Sachse, D., Tofelde, S., Niedermeyer, E.M., Strecker, M.R., Mulch, A., 2016. Elevation-dependent changes in n -alkane δ D and soil GDGTs across the South Central Andes. Earth and Planetary Science Letters 453, 234–242.
Nikrad, M.P., Kerkhof, L.J., Häggblom, M.M., 2016. The subzero microbiome: microbial activity in frozen and thawing soils. FEMS Microbiology Ecology 92, fiw081.
Nishimura, S., Yoneda, T., Fujii, S., Mukhtar, E., Abe, H., Kubota, D., Tamin, R., Watanbe, H., 2006. Altitudinal zonation of vegetation in the Padang region, West Sumatra, Indonesia. Tropics 15, 137–152.
Oksanen J, Simpson G, Blanchet F, Kindt R, Legendre P, Minchin P, O'Hara R, Solymos P, Stevens M, Szoecs E, Wagner H, Barbour M, Bedward M, Bolker B, Borcard D, Carvalho G, Chirico M, De Caceres M, Durand S, Evangelista H, FitzJohn R, Friendly M, Furneaux B, Hannigan G, Hill M, Lahti L, McGlinn D, Ouellette M, Ribeiro Cunha E, Smith T, Stier A, Ter Braak C, Weedon J (2022)._vegan: Community Ecology Package_. R package version 2.6-4.
Oton, E.V., Quince, C., Nicol, G.W., Prosser, J.I., Gubry-Rangin, C., 2016. Phylogenetic congruence and ecological coherence in terrestrial Thaumarchaeota. The ISME Journal 10, 85–96.
Pancost, R.D., Hopmans, E.C., Sinninghe Damsté, J.S., 2001. Archaeal lipids in Mediterranean cold seeps: molecular proxies for anaerobic methane oxidation. Geochimica et Cosmochimica Acta 65, 1611–1627.
Paulsen, J., Körner, C., 2014. A climate-based model to predict potential treeline position around the globe. Alpine Botany 124, 1–12.
Pester, M., Schleper, C., Wagner, M., 2011. The Thaumarchaeota: an emerging view of their phylogeny and ecophysiology. Current Opinion in Microbiology, Ecology and Industrial Microbiology / Special Section: Archaea 14, 300–306.
Peterse, F., Van Der Meer, M.T.J., Schouten, S., Jia, G., Ossebaar, J., Blokker, J., Sinninghe Damsté, J.S., 2009. Assessment of soil n-alkane δd and branched tetraether membrane lipid distributions as tools for paleoelevation reconstruction. Biogeosciences 6, 2799–2807.
Peterse, F., Prins, M.A., Beets, C.J., Troelstra, S.R., Zheng, H., Gu, Z., Schouten, S., Sinninghe Damsté, J.S., 2011. Decoupled warming and monsoon precipitation in East Asia over the last deglaciation. Earth and Planetary Science Letters 301, 256–264.
Peterse, F., van der Meer, J., Schouten, S., Weijers, J.W.H., Fierer, N., Jackson, R.B., Kim, J.-H., Sinninghe Damsté, J.S., 2012. Revised calibration of the MBT–CBT paleotemperature proxy based on branched tetraether membrane lipids in surface soils. Geochimica et Cosmochimica Acta 96, 215–229.
R Core Team, 2021. R: A language and environment for statistical computing. R Foundation for Statistical Computing, Vienna, Austria.
Raberg, J.H., Harning, D.J., Crump, S.E., de Wet, G., Blumm, A., Kopf, S., Geirsdóttir, Á., Miller, G.H., Sepúlveda, J., 2021. Revised fractional abundances and warm-season temperatures substantially improve brGDGT calibrations in lake sediments. Biogeosciences 18, 3579–3603.
Sahonero-Canavesi, D.X., Siliakus, M.F., Abdala Asbun, A., Koenen, M., von Meijenfeldt, F.A.B., Boeren, S., Bale, N.J., Engelman, J.C., Fiege, K., Strack van Schijndel, L., Sinninghe Damsté, J.S., Villanueva, L., 2022. Disentangling the lipid divide: Identification of key enzymes for the biosynthesis of membrane-spanning and ether lipids in Bacteria. Science Advances 8, eabq8652.Stieglmeier, M., Mooshammer, M., Kitzler, B., Wanek, W., Zechmeister-Boltenstern, S., Richter, A., Schleper, C., 2014. Aerobic nitrous oxide production through N-nitrosating hybrid formation in ammonia-oxidizing archaea. The ISME Journal 8, 1135–1146.
Schouten, S., Hopmans, E.C., Schefuß, E., Sinninghe Damsté, J.S., 2002. Distributional variations in marine crenarchaeotal membrane lipids: a new tool for reconstructing ancient sea water temperatures? Earth and Planetary Science Letters 204, 265–274.
Schouten, S., Hopmans, E.C., Sinninghe Damsté, J.S., 2013. The organic geochemistry of glycerol dialkyl glycerol tetraether lipids: A review. Organic Geochemistry 54, 19–61.
Sinninghe Damsté, J.S., Schouten, S., Hopmans, E.C., van Duin, A.C.T., Geenevasen, J.A. J., 2002. Crenarchaeol: the characteristic core glycerol dibiphytanyl glycerol tetraether membrane lipid of cosmopolitan pelagic crenarchaeota. Journal of Lipid Research 43, 1641–1651.
Sinninghe Damsté, J.S., Ossebaar, J., Schouten, S., Verschuren, D., 2008. Altitudinal shifts in the branched tetraether lipid distribution in soil from Mt. Kilimanjaro (Tanzania): Implications for the MBT/CBT continental palaeothermometer. Organic Geochemistry 39, 1072–1076.
Sinninghe Damste, J.S., Ossebaar, J., Abbas, B., Schouten, S., Verschuren, D., 2009. Fluxes and distribution of tetraether lipids in an equatorial African lake: Constraints on the application of the TEX86 palaeothermometer and BIT index in lacustrine settings. Geochimica et Cosmochimica Acta 73, 4232–4249.
Sinninghe Damsté, J.S., Rijpstra, W.I.C., Hopmans, E.C., Weijers, J.W.H., Foesel, B.U., Overmann, J., Dedysh, S.N., 2011. 13, 16-dimethyl octacosanedioic acid (iso-diabolic acid), a common membrane-spanning lipid of Acidobacteria subdivisions 1 and 3. Applied and Environmental Microbiology 77, 4147–4154.
Sinninghe Damsté, J.S., Rijpstra, W.I.C., Hopmans, E.C., Jung, M.-Y., Kim, J.-G., Rhee, S.-K., Stieglmeier, M., Schleper, C., 2012. Intact Polar and Core Glycerol Dibiphytanyl Glycerol Tetraether Lipids of Group I.1a and I.1b Thaumarchaeota in Soil. Applied and Environmental Microbiology 78, 6866–6874.
Sinninghe Damsté, J.S., Rijpstra, W.I.C., Hopmans, E.C., Foesel, B.U., Wüst, P.K., Overmann, J., Tank, M., Bryant, D.A., Dunfield, P.F., Houghton, K., Stott, M.B., 2014. Ether- and Ester-Bound iso-Diabolic Acid and Other Lipids in Members of Acidobacteria Subdivision 4. Applied and Environmental Microbiology 80, 5207–5218.
Sinninghe Damsté, J.S., Rijpstra, W.I.C., Foesel, B.U., Huber, K.J., Overmann, J., Nakagawa, S., Kim, J.J., Dunfield, P.F., Dedysh, S.N., Villanueva, L., 2018. An overview of the occurrence of ether- and ester-linked iso-diabolic acid membrane lipids in microbial cultures of the Acidobacteria: Implications for brGDGT paleoproxies for temperature and pH. Organic Geochemistry 124, 63–76.
Slessarev, E.W., Lin, Y., Bingham, N.L., Johnson, J.E., Dai, Y., Schimel, J.P., Chadwick, O. A., 2016. Water balance creates a threshold in soil pH at the global scale. Nature 540, 567–569.
Stieglmeier, M., Mooshammer, M., Kitzler, B., Wanek, W., Zechmeister-Boltenstern, S., Richter, A., Schleper, C., 2014. Aerobic nitrous oxide production through N-nitrosating hybrid formation in ammonia-oxidizing archaea. The ISME Journal 8, 1135–1146.
Tierney, J.E., Tingley, M.P., 2015. A TEX_{86} surface sediment database and extended Bayesian calibration. Scientific Data 2, 150029.
Tourna, M., Freitag, T.E., Nicol, G.W., Prosser, J.I., 2008. Growth, activity and temperature responses of ammonia-oxidizing archaea and bacteria in soil microcosms. Environmental Microbiology 10, 1357–1364.
Tripathi, B.M., Kim, M., Tateno, R., Kim, W., Wang, J., Lai-Hoe, A., Ab. Shukor, N.A., Rahim, R.A., Go, R., Adams, J.M., 2015. Soil pH and , 1biome are both key determinants of soil archaeal community structure. Soil Biology and Biochemistry 88–8.
Tripathi, B.M., Kim, M., Lai-Hoe, A., Shukor, N.A.A., Rahim, R.A., Go, R., Adams, J.M., 2013. pH dominates variation in tropical soil archaeal diversity and community structure. FEMS Microbiology Ecology 86, 303–311.
van der Veen, I., Peterse, F., Davenport, J., Meese, B., Bookhagen, B., France-Lanord, C., Kahmen, A., Hassenruck-Gudipati, H.J., Gajurel, A., Strecker, M.R., Sachse, D., 2020. Validation and calibration of soil δ2H and brGDGTs along (E-W) and strike (N-S) of the Himalayan climatic gradient. Geochimica et Cosmochimica Acta 290, 408–423.
Véquaud, P., Derenne, S., Anquetil, C., Collin, S., Poulenard, J., Sabatier, P., Huguet, A., 2021. Influence of environmental parameters on the distribution of bacterial lipids in soils from the French Alps: Implications for paleo-reconstructions. Organic Geochemistry 153, 104194.
Wang, C., Hren, M.T., Hoke, G.D., Liu-Zeng, J., Garzione, C.N., 2017a. Soil n-alkane δD and glycerol dialkyl glycerol tetraether (GDGT) distributions along an altitudinal transect from southwest China: Evaluating organic molecular proxies for paleoclimate and paleoelevation. Organic Geochemistry 107, 21–32.
Wang, H., Liu, W., Lu, H., Zhang, C., 2017b. Potential degradation effect on paleo-moisture proxies based on the relative abundance of archaeal vs. bacterial tetraethers in loess-paleosol sequences on the Chinese Loess Plateau. Quaternary International 436, 173–180.
Wang, H., An, Z., Lu, H., Zhao, Z., Liu, W., 2020. Calibrating bacterial tetraether distributions towards in situ soil temperature and application to a loess-paleosol sequence. Quaternary Science Reviews 231, 106172.
Wang, J.-X., Xie, W., Zhang, Y.G., Meador, T.B., Zhang, C.L., 2017c. Evaluating Production of Cyclopentyl Tetraethers by Marine Group II Euryarchaeota in the Pearl River Estuary and Coastal South China Sea: Potential Impact on the TEX_{86} Paleothermometer. Frontiers in Microbiology 8, 2077. https://doi.org/10.3389/fmicb.2017.02077.
Wang, M., Zong, Y., Zheng, Z., Man, M., Hu, J., Tian, L., 2018. Utility of brGDGTs as temperature and precipitation proxies in subtropical China. Scientific Reports 8, 194.
Weijers, J.W.H., Schouten, S., Spaargaren, O.C., Sinninghe Damsté, J.S., 2006. Occurrence and distribution of tetraether membrane lipids in soils: Implications for the use of the TEX86 proxy and the BIT index. Organic Geochemistry 37, 1680–1693.
Weijers, J.W.H., Schouten, S., van den Donker, J.C., Hopmans, E.C., Sinninghe Damsté, J. S., 2007. Environmental controls on bacterial tetraether membrane lipid distribution in soils. Geochimica et Cosmochimica Acta 71, 703–713.
Weijers, J.W.H., Panoto, E., van Bleijswijk, J., Schouten, S., Rijpstra, W.I.C., Balk, M., Stams, A.J.M., Sinninghe Damsté, J.S., 2009. Constraints on the Biological Source(s) of the Orphan Branched Tetraether Membrane Lipids. Geomicrobiology Journal 26, 402–414.
Xiao, W., Xu, Y., Ding, S., Wang, Y., Zhang, Y., Yang, H., Wang, G., Hou, J., 2015. Global calibration of a novel, branched GDGT-based soil pH proxy. Organic Geochemistry 89–90, 56–60.
Xie, S., Pancost, R.D., Chen, L., Evershed, R.P., Yang, H., Zhang, K., Huang, J., Xu, Y., 2012. Microbial lipid records of highly alkaline deposits and enhanced aridity

associated with significant uplift of the Tibetan Plateau in the Late Miocene. Geology 40, 291–294.
Yamamoto, Y., Ajioka, T., Yamamoto, M., 2016. Climate reconstruction based on GDGT-based proxies in a paleosol sequence in Japan: Postdepositional effect on the estimation of air temperature. Quaternary International, Japanese Quaternary Studies 397, 380–391.
Yang, H., Ding, W., He, G., Xie, S., 2010. Archaeal and bacterial tetraether membrane lipids in soils of varied altitudes in Mt. Jianfengling in South China. Journal of Earth Science 21, 277–280.
Yang, H., Pancost, R.D., Dang, X., Zhou, X., Evershed, R.P., Xiao, G., Tang, C., Gao, L., Guo, Z., Xie, S., 2014. Correlations between microbial tetraether lipids and environmental variables in Chinese soils: Optimizing the paleo-reconstructions in semi-arid and arid regions. Geochimica et Cosmochimica Acta 126, 49–69.
Yang, H., Xiao, W., Jia, C., Xie, S., 2015a. Paleoaltimetry proxies based on bacterial branched tetraether membrane lipids in soils. Frontiers of Earth Science 9, 13–25.
Yang, H., Lü, X., Ding, W., Lei, Y., Dang, X., Xie, S., 2015b. The 6-methyl branched tetraethers significantly affect the performance of the methylation index (MBT′) in soils from an altitudinal transect at Mount Shennongjia. Organic Geochemistry 82, 42–53.
Yang, H., Pancost, R.D., Jia, C., Xie, S., 2016. The Response of Archaeal Tetraether Membrane Lipids in Surface Soils to Temperature: A Potential Paleothermometer in Paleosols. Geomicrobiology Journal 33, 98–109.
Zeng, Z., Chen, H., Yang, H., Chen, Y., Yang, W., Feng, X., Pei, H., Welander, P.V., 2022. Identification of a protein responsible for the synthesis of archaeal membrane-spanning GDGT lipids. Nature Communications 13, 1545.
Zhang, Y.G., Zhang, C.L., Liu, X.-L., Li, L., Hinrichs, K.-U., Noakes, J.E., 2011. Methane Index: A tetraether archaeal lipid biomarker indicator for detecting the instability of marine gas hydrates. Earth and Planetary Science Letters 307, 525–534.